Journal Pre-proofs

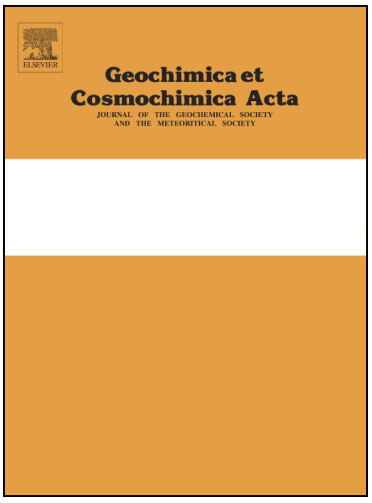

Partitioning of elements between high-temperature, low-density aqueous fluid and silicate melt as derived from volcanic gas geochemistry

M. Zelenski, A. Simakin, Yu. Taran, V.S. Kamenetsky, N. Malik

PII: S0016-7037(20)30724-9
DOI: https://doi.org/10.1016/j.gca.2020.12.011
Reference: GCA 12012

To appear in: *Geochimica et Cosmochimica Acta*

Received Date: 28 July 2020
Revised Date: 10 December 2020
Accepted Date: 15 December 2020

Please cite this article as: Zelenski, M., Simakin, A., Taran, Yu., Kamenetsky, V.S., Malik, N., Partitioning of elements between high-temperature, low-density aqueous fluid and silicate melt as derived from volcanic gas geochemistry, *Geochimica et Cosmochimica Acta* (2020), doi: https://doi.org/10.1016/j.gca.2020.12.011

Partitioning of elements between high-temperature, low-density aqueous fluid and silicate melt as derived from volcanic gas geochemistry

M. Zelenski[a,*], A. Simakin[a], Yu. Taran[b,c], V.S. Kamenetsky[a,d], N. Malik[b]

a Institute of Experimental Mineralogy, RAS, Chernogolovka, Moscow Oblast, Russia
b Institute of Volcanology and Seismology, FEB RAS, Petropavlovsk-Kamchatsky, Russia
c Institute of Geophysics, UNAM, Coyoacan, Ciudad de Mexico, Mexico
d School of Natural Sciences, University of Tasmania, Hobart, TAS, Australia

** Corresponding author. E-mail address: volcangas@gmail.com (M. Zelenski)*

Abstract

By comparing high-quality volcanic gas and whole rock compositions, we calculated the apparent (observed) mass partition coefficients *Kd** for 58 elements on six basaltic volcanoes located in arc and rift/hotspot settings. The inferred *Kd** vary from ~1100 for sulfur to 0.0001 for zirconium, i.e., within seven orders of magnitude. Only 14 elements have *Kd** >1, including highly volatile S, Se, Te and halogens,

as well as Tl, Re, Os, Bi, Cd, Au, In and As. Alkali metals have *Kd** in the range from 0.1 for Cs to 0.01 for Na. Partition coefficients of other rock-forming elements are < 0.001. The partition coefficients for elements depend on element speciation and concentrations of ligand-forming elements in the gas such as sulfur and chlorine. Elements transported in the gas predominantly as halides have higher partition coefficients in HCl-rich arc gases, whereas elements preferably forming sulfides, hydrides and free atoms, have higher *Kd** in sulfur-rich, HCl-poor and reduced rift/hotspot gases. Degassing directly from the free melt surface is negligible; deep gas passing through the erupting vent is quickly overwhelmed by the signal of low-pressure degassing. Equilibration of rising bubbles with the surrounding melt almost eliminates the difference between *Kd** calculated for degassing lava flows (no connection with deep magma) and for lava lakes (convective mass exchange with deep magma takes place). Diffusion does not strongly affect the apparent partitioning of magmas degassing at surface. Gas bubbles growing in near-surface silicate melts at atmospheric pressure have a large density difference compared to the surrounding melt of 12– 15 thousand times. This leads to the rapid expansion of such bubbles and a decrease in the thickness of the diffusion boundary layer in the melt due to its stretching around the growing bubble, which sharply decreases diffusion fractionation. As a result, the apparent partition coefficients (*Kd**) for degassing basaltic volcanoes are close to the equilibrium ones (*Kd*) for most of the elements. The partition

coefficients of volatile elements (S and Cl) calculated from the comparison of volcanic gas and rock compositions are in agreement with the values determined previously via experiments or theoretical modeling.
Keywords: element partitioning; volcanic gas; silicate melt; bubble growth; diffusion; equilibrium

1. Introduction

Aqueous fluids exist over a wide range of temperatures, pressures, and densities and play a key role in element transport and distribution at the Earth's surface, in the crust, and in the upper mantle due to fluid mobility and transport properties. Near-surface, low-density (0.15 to 0.6 kg/m^3 at atmospheric pressure), water-rich fluids at temperatures from ~80 to 1200 °C are conventionally referred to as "fumarolic gases" and "eruptive volcanic gases". Volcanic and fumarolic gases have been extensively studied during recent decades in terms of their physical parameters and chemical composition, including major gas species, rare gases, and isotopic ratios (e.g., reviews by Symonds et al., 1994; Fischer and Chiodini, 2015). Similarly to more dense (crustal) fluids, volcanic and fumarolic gases contain some amounts of trace elements (which include metals and metalloids) that are transported to the surface and discharged into the atmosphere. The total emission of trace elements with eruptive and fumarolic gases is significant and affects the distribution of elements on the planet (e.g., Nriagu, 1989; Hinkley et al., 1999; Mather, 2015). This is especially noticeable for some rare volatile elements (As, Se, Te, Re, Cd, Tl, and Bi) that show high enrichment in volcanic gases.

Despite many publications on the topic, many aspects of the composition of volcanic gases remain poorly understood. In particular, the trace element patterns of volcanic gases and volcanic aerosols (condensed gases and silicate rock particles) drastically differ for different volcanoes with the dispersion of data exceeding four orders of magnitude for a certain element at similar degassing conditions (see for example Fig. 16 in Zelenski et al., 2013) and even at the same volcano and the same sampling site, e.g., over basaltic lava flows of Kilauea volcano (cf. Olmez et al., 1986; Crowe et al., 1987; Hinkley et al., 1999; Mather et al., 2012). The reason for these large discrepancies is rarely discussed but may arise from inaccuracies in the sampling and analytical procedures for elements in vanishingly low concentrations rather than reflect real fluctuations in the gas compositions. Given such scatter in the initial data, estimates of global volcanic emission of trace elements likely contain significant uncertainties.

There is no answer on the question whether trace and some major (Cl, S, F) elements in the gas phase are in equilibrium with the silicate melt during surficial degassing of lava flows and lava lakes. Gas-to-melt concentration ratios for such systems were presented, however, in several recent articles (Pokrovski et al., 2013; Zelenski et al., 2014; Mather, 2015, Gauthier et al., 2016) without discussing element volatilization and equilibration. In a number of works, element speciation in volcanic gases and

volcanic gas – silicate rock systems was considered from the perspective of equilibrium thermodynamics, assuming that equilibrium in the studied systems has been attained (e.g., Symonds et al., 1992; Symonds and Reed, 1993; Wahrenberger, 1997; Churakov et al., 2000; Taran et al., 2001).

However, the equilibrium hypothesis is not necessarily applicable for real systems due to slow diffusive transport of components from the melt to the gas – melt interface. Diffusion of species in silicate liquids, even at magmatic temperatures, is a slow process (Zhang et al., 2010). In the case of magma degassing, the most important difference is between water, with its high diffusivity, and almost all other elements and species with diffusion coefficients one – two orders of magnitude lower. Significant diffusion fractionation of volatile elements was observed during degassing from the surface of artificially made dry silicate melts in laboratory conditions (MacKenzie and Canil, 2008; Johnson and Canil, 2011). Researches also demonstrated that partial evaporation of volatile components from the silicate melt is not limited by reaction kinetics at the gas–melt interface and is controlled mainly by diffusion (e.g., Beerkens, 2001; Lenoir et al., 2010; van Limpt et al., 2011).

In this paper we demonstrate via numerical modeling of diffusion transport in silicate melts at atmospheric pressure that the rapid expansion of low-density gas bubbles and a decrease in the thickness of the diffusion boundary layer reduces the diffusion fractionation. The modeling also showed that the combination of diffusion fluxes of different elements and species toward a bubble growing within near-surface silicate melt may result in a gas composition that is almost indistinguishable from the equilibrium composition. Considering the modeling results, we assumed that the compositions of volcanic gases at the moment of separation from the silicate melt are close to equilibrium compositions and, therefore, concentration ratios for elements in the volcanic gas – silicate melt system can be described in terms of equilibrium partition coefficients. For calculations, after critically evaluated published data on the trace-element composition of volcanic gases and volcanic rocks, we selected data for six basaltic volcanoes of different tectonic settings. As a proxy for the compositions of the melts, we used data on the rock analyses of those eruptions during which gas samples were collected, taking into account the possible loss of volatile elements by basaltic melts during degassing (Lambert et al., 1985; Pennisi et al., 1988). Then, we discuss the systematic differences in the partition coefficients calculated for volcanoes from different tectonic settings and the difference between volcanic gases exsolved from ~~surficial~~ lava flows and from convective lava lakes. Our study provides new insight into volcanic degassing and its impact on Earth's atmosphere and the global circulation of elements.

2. Terminology and assumptions

A list of the symbols used in this article is presented in Table 1. Below are some comments on general terms and symbol usage that require more explanation.

(1) Partitioning of an element or a chemical species X between two coexisting phases A and B in the state of equilibrium obeys the Berthelot – -Nernst distribution law (Berthelot, 1872; Nernst, 1891) and, in its simplest notation, is expressed by concentration ratio of (X) between both phases:

$$Kd = C_X^A / C_X^B \quad (1).$$

The concentration ratio Kd is called a partition or distribution coefficient. A certain inconsistency in the geological literature in the use of the terms "partition coefficient" and "distribution coefficient" was discussed in a special scientific comment by Beattie et al. (1993). In geological applications, both terms are in use. As recommended by Beattie et al., we use the term "partition coefficient" throughout the paper. "*Kd*" was applied for partition coefficient whereas the symbol "*D*" in this article is reserved for diffusivity. The symbol "*Kd*" stands for the equilibrium partition coefficient, whereas *Kd** designates the effective (i.e., apparent or observed) partition coefficient.

(2) We use in the text closely related the terms "magma", "lava" and "silicate melt", so the clarification is needed. This article deals only with silicate melts. Magma indicates deep silicate melt saturated with several % of volatile components, typically in a vertical conduit; whereas lava designates a partially degassed silicate melt at the surface, containing residual volatiles at a level of 0.2 –0.3 wt. % H_2O. The degassing of such surficial melt continues until it solidifies. The terms "magma" or "lava" as a part of complex terms (magma conduit and lava flow) were used in cases where it was necessary to emphasize the shape or location of the object (vertical magma column, subhorizontal lava flow).

When we discuss only physical processes, such as diffusion, we often use the term "silicate melt". The use of the term "silicate melt" is also justified because the partitioning of elements occurs at most between the melt and the gas, and phenocrysts present in magma or lava participate little in the exchange of elements due to slow diffusion rates in crystals. We study partitioning of elements between volcanic gas and silicate melt keeping in mind, that the composition of bulk magma or lava is slightly different from that of the silicate melt.

(3) Saying here "surficial and near-surface silicate melts" we mean that such melts have a free surface (gas–melt interface) exposed to the atmosphere, the degassing occurs at the atmospheric pressure (~0.05-0.1 MPa depending on the local elevation). We assume that the pressure change within the thickness of the basaltic lava flow has little effect on the degassing process and can be neglected, so that the nucleation and diffusion-driven growth of bubbles in a subhorizontal lava flow occurs under approximately isobaric conditions.

(4) The terms "volcanic gas" and "low-density surficial aqueous fluid" are equal to each other. Only gases exsolved from surficial basaltic melts were considered in this study for estimation of partition

coefficients. Fumarolic gases were not taken into account because of the unknown element deposition from the gas during its ascent along a fumarolic duct.

(5) Concentrations in equations are expressed as non-dimensional mass fraction (parts per unity).

3. Are volcanic gases in equilibrium with melt?

The term "equilibrium partitioning" makes sense only if coexisting phases (e.g., gas and melt) are in equilibrium or closely approach it. Before we calculate partition coefficients for the volcanic gas – silicate melt system, a key question should be answered: are element concentrations in the volcanic gas close to equilibrium with the melt? Below we consider this issue for three different ways of the melt degassing: (1) degassing from the free surface of the melt, (2) degassing through bubble growth and ascent in a subhorizontal surficial lava flow, and (3) a special case is considered for inherited bubbles, the nucleation and primary growth of which occurred in a vertical magma column in the decompression mode, and further ascent of such inherited bubbles to the melt surface takes place in approximately isobaric conditions in a horizontal lava flow. The term "melt" in cases (1) and (2) refers to partially degassed silicate melt containing 0.2-0.3 wt. % residual water and other volatiles, which is characteristic of surficial lava flow or sub-surface lava in a lava tube. The parameters of such melts are listed in Table 2. Silicate melt in a vertical conduit may contain more volatiles, depending on the lithostatic pressure.

3.1. Degassing from the free melt surface directly to the atmosphere

Here, we evaluate the contribution of diffusive degassing from the free melt surface directly into the atmosphere to the total gas escape from a lava flow; the advective transport of components via bubbles is discussed below in Section 3.2. Degassing from the free surface of the silicate melt in an open system can be described in three steps (from van Limpt et al., 2011, adapted for the natural silicate melts): (1) diffusive transport of volatile species to the gas–melt interface; (2a) evaporation of volatile species dissolved in the melt from the gas–melt interface and (2b) chemical reactions of the gaseous species with non-volatile components of the melt at the gas–melt interface; and (3) diffusive or convective transport of the volatile gaseous species from the gas–melt interface into the open air.

It is believed that, at least in the glass production in industry, reactions at the gas – silicate melt interface are fast and that equilibration at the glass–gas melt interface occurs in a time negligible compared to diffusion equilibration (Cable, 1978; Beerkens, 2001; van Limpt et al., 2011). Consequently, the escape of volatile components from the melt is limited by the diffusion. As follows from the steps (1) – (3), two conjugated diffusive boundary layers are formed during melt evaporation, one in the melt and the second in the adjacent gas. The gas–side boundary layer has a significant effect on both mass transfer and the composition of gases separated from the melt. The presence of non-zero concentrations of volatile components from the gas–phase side reduces the diffusion flux of these components from the melt. The

exact solution of the diffusion problem for two conjugated diffusion layers requires considering many factors: the changing concentrations of components at the interface, the presence of free or forced convection at the gas–phase side, and this, ultimately is complex.

The simplified approach, which is applied in the present article, considers the limiting case when the thickness of the gas–phase boundary layer is equal to zero. In this case, the diffusion flux from the melt is maximal, and we obtain an upper estimate. A situation close to the limiting case is realized, for example, if the gaseous boundary layer over lava is blown away by an air stream (wind). The melt, from the surface of which, all exsolved gas is immediately blown off, is an open system.

Degassing from the surface of the silicate melt with zero thickness of the gas–phase side boundary layer corresponds to the classic non-stationary diffusion problem of a semi-infinite medium with surface maintained at a zero level (e.g., Crank, 1975). The initial condition for such calculations is the homogeneous melt; this corresponds to the moment when the melt reaches the Earth's surface, forming a lava flow. We have performed a numerical simulation of this process using the explicit control–volume method for semi-infinite medium with a flat boundary (see Annex 1). According to the model, the contents of volatile species in the gas emitted from the free melt surface do not depend on the gas–melt partitioning and are completely determined by the initial concentrations and diffusivities of these species in the melt:

$$C_X^{fl} \approx X/H_2O = \frac{C_X^{melt}}{C_W^{melt}} \times \sqrt{\frac{D_X}{D_W}} \qquad (2)$$

A diffusion-controlled open-system degassing from the free melt surface closely matches laboratory experiments on degassing the melt into a free atmosphere at a pressure of 1 bar (Johnson and Canil, 2011).

The same equation can be obtained from the analytical solution of the non-stationary diffusion problem of a semi-infinite medium. Crank (1975) in the book "Mathematics of Diffusion" provides the following equation for the flux of a component diffusing from a semi-infinite medium:

$$q = \left(D \frac{\partial C}{\partial x} \right)_{x=0} = \frac{C_0 \cdot \sqrt{D}}{\sqrt{\pi t}} \qquad (2a),$$

where q (kg/m^2) is the component flux, and C_0 (kg/m^3) is the initial concentration of the diffusant in the medium while the surface is maintained at a zero level. If we take two components, one of which is water, then we obtain an equation for the concentration of this diffusant in the exsolving fluid, which coincides with Eqn. 2:

$$C_X^{fl} \approx \frac{q_X}{q_W} = \frac{C_X^{melt}}{C_W^{melt}} \times \sqrt{\frac{D_X}{D_W}} \quad (2b).$$

Equation 2 is valid only if the surface concentrations of the exsolved volatile components are maintained at the zero level (the hypothetical limiting case). In reality, at a nonzero thickness of the gas–phase boundary level, the composition of the gas separating from the melt is intermediate between the composition determined by Eqn. (2) and the equilibrium composition.

The relative contribution of the degassing from the free melt surface to the total volcanic gas flux can be estimated from the equation for the total amount *M* of a diffusant that has left the melt at time *t* per square unit in the case of the non-stationary diffusion from the semi-infinite medium with the surface maintained at a zero level (Crank, 1975):

$$M = 2C_0 \frac{\sqrt{Dt}}{\sqrt{\pi}} \quad (3),$$

where M is expressed in kg. If we substitute values of D_{H2O} and $C_{H2O,}$ (the melt parameters are taken from Table 2 for Tolbachik), then we find that only ~0.57 g/m^2 of H_2O may be released during the first 1000 seconds of degassing from the free melt surface. This time is comparable with the lifetime of the lava flow before it rests. Such an amount of water is contained in 1 m^2 of the melt layer of 0.08 mm thickness; an extremely thin layer compared to the thickness of the whole lava flow.

The degassing rate observed on natural lava flows is several orders of magnitude higher than the degassing directly from the surface calculated as above. This can be illustrated by the following example. The lava flow of the 2013 Tolbachik eruption was intensely emitting gas, when it passed through a lava tube of about 1000 m long. Almost all the gas leaving the melt discharged through a skylight (hornito) with a cross-section of about 10 m^2 at a speed ~5 m/s, which corresponds to ~50 m^3/s. With the water vapor content in the gas of about 50% and a temperature of 1065 °C (Zelenski et al., 2014), the total emission of H_2O through the skylight can be estimated at ~4.5 kg/s. If the average width of the lava flow is taken to be 5 m (as was observed), then the area of the degassing surface will be about 5000 m^2, which results in the degassing rate of about 0.9 g/m^2 per second. This amount is more than three orders of magnitude higher than the gas release directly from the surface calculated from Eqn. 3 (0.57 g/m^2 per 1000 s). This example clearly indicates that the main form of degassing of the surficial silicate melt (> 99.9 %) is advection of gas bubbles.

3.2. Degassing via advection of gas bubbles and diffusion control on *Kd**

Separation of the major amount of volcanic gas from the lava flow occurs by bubbles in two stages: (1) bubble nucleation and growth under diffusion control, and (2) the coalescence of small bubbles into

large ones and the rise of large bibles to the melt surface (Bottinga and Javoy, 1991; Mangan et al., 1993; Cashman et al., 1994; Gaonac'h et al., 1996a, b). The formation of large bubbles is important because only large bubbles can reach the surface of the lava flow and unload the gas into the atmosphere. The ascent velocity u of a bubble in the Stokes regime (Reynolds number Re << 1) is proportional to the square of the bubble diameter (e.g., Lamb, 1932):

$$u = \frac{2}{9}\frac{\left(\rho_{melt} - \rho_{fl}\right)}{\eta} gR^2 \qquad (4),$$

where g is the gravitational field strength (m/s^2); R is the radius of the bubble (m), ρ_{melt} and ρ_{fl} are the mass densities of the melt and bubbles, respectively (kg/m^3); and η is the dynamic viscosity (kg/(m·s). For example, a bubble with a size approximated by a sphere with a radius of 20 mm has a rise velocity of about 5 cm/s in the lava of Kilauea volcano with the parameters listed in Table 2, without leaving the Stokes' regime (Reynolds number ~0.08). The successive coalescence of small bubbles into large ones ("cascading coalescence", Gaonac'h et al., 1996a) eventually results in large bubbles that are capable of reaching the surface in a short time. In comparison, bubbles of 0.1–1 mm have an ascent rate of the order of 10^{-5}–10^{-3} cm/s and are retained in the melt throughout the lifetime of the lava flow. This includes small fluid bubbles that have been formed at shallow depth in a conduit (vertical magma column) and bubbles that have nucleated in a surficial lava flow.

Diffusivities of magmatic volatiles and metals in a silicate melt vary within two to three orders of magnitude for a silicate melt of a given composition at a given temperature (Zhang and Stolper, 1991; Brady, 1995; Baker and Balcone-Boissard, 2009; Zhang et al., 2010; Zhang and Cherniak, 2010; Zhang and Ni, 2010; Ni and Zhang, 2018, and references therein). Water diffusion is by far faster than the diffusion of almost all other elements or species, with the exception of Li and Na. Because the diffusivities are so different, one can expect that some components diffuse into a growing bubble fast, whereas other components diffuse slowly, thus causing diffusion fractionation and preventing attainment of equilibrium in the volcanic gas – silicate melt system. Therefore, the observed Kd^* calculated on the basis of gas and melt compositions may differ from the equilibrium values. However, for surficial and near-surface degassing under low (atmospheric) pressure, we have a special case. As we show below (please refer to Annex 1 for further details), low fluid density and large bubble expansion significantly weakens the diffusion fractionation during the bubble growth in a surficial silicate melt.

For the fluid-melt system, Equation (1) can be rewritten as:

$$Kd = C^{fl}_{X,eq} \Big/ C^{m}_{X,eq} \qquad (5)$$

where the subscript eq means that the fluid–melt system is in equilibrium. The measured partition coefficient

$$Kd^* = C^{fl}_{X,meas} \Big/ C^{m}_{X,meas} \qquad (6)$$

can be constrained by the relative (against water) diffusion rates of components in the melt. In the case of the diffusion into essentially static bubble (Peclet number Pe <<1) at the small degree of vesiculation, the effective (measured) fluid–melt partition coefficient $Kd^* = C_X^{fl} / C_X^m$ can be expressed a function of the equilibrium coefficient *Kd* as follows:

$$Kd^* = \frac{Kd \cdot \bar{D}_X}{Kd \cdot \Delta C_W + \bar{D}_X}; \ \bar{D}_X = D_X / D_W \qquad (7),$$

where *Kd* stands for the equilibrium partition coefficient, *Kd** is the effective partition coefficient, ΔC_W - the water oversaturation expressed as a non-dimensional mass fraction, and D_X and D_W are the diffusion coefficients for component *X* and for water, respectively.

It can be also shown (Annex 1) that diffusion fractionation is significantly decreased for bubbles with density of the order of 0.15 – 0.20 kg/m^3, growing in the near-surface silicate melt with nonzero supersaturation in water ΔC_W . During the growth of such bubbles, the diffusion boundary layer in the melt is thinning due to the stretching of the melt around the bubble. For example, the melt layer with thickness δh and volume δV in the direct contact with the bubble becomes thinner by four times with doubling of the bubble diameter. Thinning of the boundary layer increases the diffusion flux of metals into the bubble. When the ratio of partial water densities R_ρ in the melt and in the fluid

$$R_\rho = \Delta C_W^{melt} \cdot \rho_m / C_W^{fl} \cdot \rho_{fl} \approx \Delta C_W^{melt} \cdot \rho_m / \rho_{fl} \qquad (8)$$

is larger than about 10, the effect of the bubble expansion becomes important. For Tolbachik, ΔC_W^{melt} = 0.27 wt. % H_2O results in R_ρ= 0.0027×2700/0.184 ≈ 35. For Kilauea, $R_\rho \approx$ 32, thus in both cases, the expansion-derived stretching of the melt should be taken into account. We demonstrated, using an approximate analytical solution and numerical modeling by mesh-less inverse multi-quadric method (Annex 1), that a boundary layer with the sharp exponential concentration profile with large gradient is formed near the bubble boundary, which accelerates diffusion and leads to the dependence of diffusion flux $q \propto \sqrt{D}$. Then *Kd** becomes:

$$Kd^* = \frac{Kd \cdot \sqrt{\bar{D}_X}}{Kd \cdot \Delta C_w + \sqrt{\bar{D}_X}} \qquad (9)$$

Expression (9) has two limits. At small *Kd*, the diffusion flux is sufficiently fast to effectively transport component X from the melt into the bubble. Then, we can neglect with term $Kd \cdot \Delta C_w << \sqrt{\bar{D}_X}$ and the effective *Kd** becomes equal to the equilibrium *Kd.* At low water contents of 0.2–0.3 wt. %, which are characteristic of surface lava lakes and lava flows, the term $Kd \cdot \Delta C_w$ is also small for the majority of elements and *Kd** differ little from *Kd*. In the opposite case, when $Kd \cdot \Delta C_w >> \sqrt{\bar{D}_X}$, we can neglect

$\sqrt{D_X}$ and $Kd^* = \sqrt{D_X}/\Delta C_w$: the observed partition coefficient is directly proportional to the square root of the diffusivity ratio and inversely proportional to supersaturation in water.

The low water content in surficial silicate melt leads to another effect that weakens the fractionation of elements. When the concentration of water < 1 wt. %, its speciation changes from the predominantly molecular form H_2O to the OH form (e.g., Stolper, 1982; Zhang et al., 2017; Ni and Zhang, 2018). At water contents of 0.2–0.3 wt. % characteristic of surficial basaltic melts, the diffusion rate of water in the form of OH decreases by a factor of three compared to the diffusion rate of water at 4 wt. % H_2O (Zhang et al., 2017; Ni and Zhang, 2018). A decrease in the water diffusion rate in a low-water silicate melt further expands the list of elements whose concentrations in gas bubbles are close to equilibrium concentrations.

The combination of the described processes results in the fact that the measured partition coefficients of the elements between the volcanic gas and the melt $Kd^* = C_X^{fl}/C_X^{melt}$ are almost equal to the equilibrium partition coefficients *Kd* (Fig. 1a). At least, this is true for elements with $Kd \leq 20$ ($\log Kd < 1.3$) which comprises the majority of trace elements in the volcanic gas except for Se and Te. This effect is only relevant for the surficial degassing and has no importance for decompression degassing at greater depths, during which dense fluid bubbles grow in the melt. However, Fig. 1b also shows that even without taking into account the effect of rapid expansion, $Kd^* = C_X^{fl}/C_X^{melt}$, a significant difference between the apparent Kd * and equilibrium Kd is achieved only for the most volatile elements, for which Kd> 1 ($\log Kd \geq 0$).

3.3. Diffusion boundary layer and diffusion distance into the bubble

The significant decrease in diffusion fractionation, as described in Section 3.2., is based on the fact that a diffusion boundary layer is formed around the growing bubble, through which diffusion occurs in a stationary mode. The thickness of the diffusion boundary layer depends on the Peclet number for a given element and a given bubble and ranges from a few μm to several tens of μm. A we show below, for elements with a partition coefficient $Kd \leq 1$, the presence or absence of the diffusive boundary layer has no substantial effect, because the characteristic distance of diffusion from the melt into the bubble for such elements is very small. Only elements with $Kd > 1$ are affected by the diffusive boundary layer.

Let us determine the thickness of the melt layer surrounding the bubble, which contains the number of atoms required to equilibrate a bubble with respect to the element of interest. The thickness *h* of the required melt can be calculated using the following equation:

$$h = \frac{r_b}{3} \cdot \frac{\rho_{fl}}{\rho_m} \cdot Kd \qquad (10),$$

which may be re-written for Tolbachik melt as $h = 1.14 \cdot 10^{-5} \cdot Kd$. For partition coefficient $Kd = 0.1$ and $r_b = 0.5$ mm, the thickness of the melt layer is about 10^{-6} mm (10Å), i.e. approximately five to six monoatomic layers. The characteristic timescale a^2/D for diffusion at such distance for silicate melt at 1000–1200 °C is of the order of 10^{-5}–10^{-6} s, which means that, at any moment, the growing bubbles have enough time to come to equilibrium with the melt in respect to elements with low partition coefficients (Kd ≤ 0.1).

For elements with Kd <0.02 (for example, Na, Al, Ca, Fe, Ba, and Zr, see Section 5.2.), formal application of formula (10) gives the thickness less than monoatomic layer, which is impossible from the physical point of view. This makes the formal calculation of diffusion equilibration meaningless. The rate of transition of such elements from the melt into the fluid at the fluid-melt interface is apparently determined by other processes, such as the physical evaporation of molecules of a volatile compound (for example, NaCl) or a chemical reaction of a non-volatile component of the melt with fluid (for example, $FeO(m) + 2HCl(fl) = FeCl_2(fl) + H_2O(fl)$).

The observed partition coefficients *Kd** (for those cases where they are justified from a physical point of view, i.e., for $Kd \geq 0.1$) can be calculated numerically for a growing bubble if the equilibrium partition coefficients *Kd* are known (Annex 1). Calculations for a Tolbachik gas–melt system showed that the observed *Kd** are somewhat lower than the equilibrium *Kd*: Br – by 1.5%, Cd – by 5.5%, Tl – by 12%, Te – by 40%. For the Kilauea volcano, the observed *Kd** for Tellurium is less than the equilibrium value by 60% (2.5 times). For elements with $Kd < 1$ (see Table 5), the observed and equilibrium partition coefficients are almost the same.

3.4. Transition from decompression to steady state isobaric growth mode

Bubbles may nucleate in a surficial lava flow under isobaric conditions at low water supersaturation. However, the majority of small bubbles existing in the lava flow nucleate earlier at greater depths in rising magma (Bottinga and Javoy, 1991; Mangan et al., 1993; Cashman et al., 1994), where they grow during the magma ascent both due to decompression and diffusion (e.g., Sparks, 1978; Bottinga and Javoy, 1991). In the absence of direct measurements, the metals concentrations in such bubbles are difficult to estimate, because the partition coefficients for the fluid–melt system crucially depend on the volume concentrations of major species (CO_2, H_2O, SO_2, H_2S, and HCl), which rapidly change during the decompression (e.g., Witham et al., 2012). This means that at the moment the melt enters the isobaric zone (a surficial lava flow), trace-element concentrations in fluid bubbles can be randomly higher or lower than the equilibrium trace-element concentration for surficial (low-pressure isobaric) conditions.

These random concentrations asymptotically tend to equilibrium concentrations, characteristic of the surficial silicate melt. This may cause a gain in metals or, conversely, the solution of excess metals back into the melt. For the asymptotic approach of the initial (random) and the final (surficial)

concentration of the element of interest, the transition time can be designated as the time during which the initial difference between the random and the surficial concentration decreases by some pre-defined value, for example, by an order of magnitude. With this definition, the transition time depends on the element and melt properties and the bubble initial diameter, but not on the initial concentration of the element in the bubble.

We performed numerical calculations of the transition time from the decompression to the isobaric growth modes using the explicit control-volume method (Annex 1). Such calculations are approximate, since we did not take into account the inhomogeneity of the concentration field around the bubble, which appeared earlier during the growth of the bubble in the vertical magma conduit in the "decompression - diffusion" mode. The calculated transition time is proportional to the square of the bubble diameter and inversely proportional to the element diffusivity. For a 1-mm bubble, the transition times range from fractions of microseconds to several minutes (Table S3, Annex 1). This indicates that upon transition from the decompression-diffusion growth mode to the isobaric (purely diffusion) growth mode, small bubbles with the diameter of ~1 mm or less quickly "forget" their initial compositions and become identical to the bubbles that have nucleated and grown in the isobaric surficial lava flow. With an increase in the size of the bubble, the equilibration time rapidly increases. However, large bubbles usually leave the melt during the eruption directly at the erupting vent due to their large Stokes ascent rates, and only small bubbles are retained in the lava flow.

It follows from the said above that the gas emitted directly from the eruptive vent may differ in its trace-element composition from the gas emitted from lava flows and lava lakes. However, the measured compositions of gases released from a lava flow and from an open degassing volcanic vent, differ little (see Discussion, Section 6.4.). Apparently, re-equilibration of the trace-element composition with melt in bubbles of ~10 mm in diameter or more is also fast enough.

3.5. A short summary of equilibration in the volcanic gas – silicate melt system

(1) Degassing from the free melt surface is a non-equilibrium process, in which the element flux through the melt surface is proportional to the concentration of an element in the melt and to the square root of the element diffusivity. The relative contribution of degassing from the free surface of a lava flow is less than 0.1% and can be neglected.

(2) The nucleation, growth, and ascent of bubbles is the primary way of degassing a surficial lava flow. Low density of the fluid at low ambient pressure results in increased bubble expansion, which significantly reduces the diffusion fractionation due to stretching and thinning the diffusion boundary layer around the bubble. For most elements, the observed and equilibrium partition coefficients in the volcanic gas – silicate melt system do not differ significantly.

(3) Transition from the decompression to the isobaric growth mode occurs during seconds or fractions of seconds for small bubbles (≤1 mm). During this transition, the bubble "dumps" excess metal back into the melt, or, conversely, quickly gains the trace-element concentrations. After the transition, the bubble “forgets” their initial concentrations and becomes indistinguishable from bubbles that nucleated and grew solely in isobaric conditions.

4. Input data for the calculation of partition coefficients between volcanic gas and silicate melt

As experimental data on the partition coefficients for low-density fluids (volcanic gases) are not available, the partition coefficients in the volcanic gas – silicate melt system can be only determined using data on natural objects. For this purpose, we prepared a credible dataset of element concentrations both in volcanic gases and rocks for four arc and two rift/hotspot volcanoes. We also considered differences in the temperature and concentrations of major gas species (SO_2, H_2S, and HCl) in emissions from volcanoes located in arc and rift/hotspot tectonic settings.

4.1. Volcanic gas composition

Although several dozen studies on trace-element compositions in volcanic gas have been published, only a few of them contain data suitable for calculating the partition coefficients. We selected four arc and two rift/hotspot basaltic and basaltic andesite volcanoes taking into account the following criteria. (1) Degassing occurs directly from subaerial silicate melt (lava flow or lava pond) or from very shallow magma in a subsurface lava lake or a conduit. Consequently, all fumarolic data were excluded. Only in this case we can expect zero or only small input or depletion in elements along the gas path to the surface due to secondary processes, including the deposition of trace elements due to cooling of the gas; minimal contributions from low-temperature hydrothermal systems on volcanoes that often contain much boron and arsenic; and entrainment of wall rock particles, typically particles of altered rocks (Symonds et al., 1992; Hedenquist, 1995; Henley and Berger, 2013). (2) The explosive fragmentation of magma is negligible, i.e., the amount of silicate aerosol in the gas is as low as possible. (3) The melt has low viscosity, which ensures fast bubble rising and intense degassing.

The listed criteria correspond to basaltic and basaltic andesite volcanoes in a state of continuous effusive eruption (Kilauea, Mather et al., 2012; Tolbachik, Zelenski et al., 2014), open-vent or lava pond degassing (Etna, Aiuppa et al., 2003; Ambrym, Allard et al., 2016; Masaya, Martin et al., 2012) or the degassing of a near-surface lava lake through a spatter cone (Erta Ale, Zelenski et al., 2013). Analyses of volcanic gas from selected volcanoes have reasonably low dispersion in trace element abundances. Emissions from Erebus, Stromboli, and Holuhraun (e.g., Zreda-Gostynska, 1997; Allard et al., 2000; Gauthier et al., 2016) were also preliminarily considered but were not used in further calculations because the results were inherently different from the other six volcanoes studied. General information regarding

the volcanoes under the study, including the major gas species, is given in Table 4. The molar abundances of H_2O, S and HCl in gases of the six selected volcanoes are shown in Fig. 2. The compiled and corrected data on trace element abundances in volcanic gases are provided in Annex 2, Supplementary Table S2.

After representative analyzes were selected, we calculated the fraction of silicate aerosol ("weight ash fraction" as suggested by Aiuppa et al., 2003) in the gas analyses using the formula

$$\mathrm{WAF} = \frac{(C_X/C_R)_{rock}}{(C_X/C_R)_{gas}} \quad (11),$$

where X stands for the element of interest and R is the reference element with low volatility. In this notation, the weight ash fraction (WAF) may change from 0 to 1. Aerosol fractions were subtracted from the measured concentrations by multiplying the measured concentrations by the calculated WAF values. As a reference element, we used ytterbium because it is an element with low volatility, which can be easily detected by conventional ICP-MS analysis and because it was present in the datasets for all selected volcanoes. In such a way we obtained concentrations of elements that were initially emitted as gaseous species:

$$C_{gas\_emission} = C_{meas} \times (1 - WAF) \quad (11a).$$

We took into account that in some datasets, the weight ash fractions were already subtracted by authors. Thus, only gas compositions purified from silicate rock aerosol were used for the comparison with rock compositions.

4.2. Silicate melt composition

The composition of silicate melt can be reasonably approximated by bulk analyses of the corresponding rock, with the correction for losses of volatile elements (B, Cd, Se, Re, and Bi) during degassing. Such correction is necessary for the most volatile elements, unless they are measured in quenched glasses. Correction was performed on the basis of emanation coefficients (Lambert et al., 1985), which show how much of the element is expelled from the silicate melt before it solidifies into massive rock. Emanation coefficients for B, Se and Cd were taken from Rubin (1997) and for Re and Bi from Lassiter (2003) and Norman et al. (2004). Correction for losses for elements having emanation coefficients < 10%, such as Te and Tl, has little sense because of its small influence on the calculated Kd (Rubin, 1997). Preferential concentration of some elements in early phenocrysts also affects the concentrations of elements in the melt. However, the amount of early phenocrysts in the quenched basaltic scoria is commonly small and rarely exceeds 2–4 wt. %. Phenocrysts are mainly represented by olivine and rare chromite crystals, and

therefore have little effect on the bulk trace element composition of the melt, especially with respect to incompatible volatile elements. Overestimated or underestimated concentrations of elements in rock analyses as well as possible outliers were corrected by comparison with similar rocks from other volcanoes in the same way as it was done for volcanic gas analyses. The correction of rock compositions for the six selected volcanoes is described in detail in Annex 2; the corrected data on element abundances are provided in Supplementary Table S1.

The selected analyses of lavas and scoria from six volcanoes in this study contain SiO_2 from 44.5 to 53 wt. % and total alkalis $K_2O + Na_2O$ from 2.5 to 6 wt. %, which places these rocks into basalt, basaltic andesite and trachybasalt fields on the total alkali vs. silica (TAS) diagram (Fig. 3). Concentrations of all elements expressed in ppm, including rock-forming and trace elements, are shown on the spider diagram in a logarithmic scale, in descending order of concentration (Fig. 4). The difference in rock compositions between arc rift/hotspot basalts is clearly visible. Arc-related basalts are enriched in incompatible lithophile elements, some chalcophile elements (Cu, As, Ag, Pb, and Bi), and chlorine and depleted in Cr, Ni, Nb, Ta, S and Se.

5. Trace elements in volcanic gases compared to volcanic rocks

5.1. Gas and rock side-by-side comparison

The relations between element concentrations in silicate melt (approximated by the bulk rock analyses) and in coexisting fluid (volcanic gas) can be represented on a plot (Fig. 5). The diagram shows that for many studied elements, a broad correlation exists between the measured concentrations of elements in volcanic gas and in corresponding volcanic rock. For some elements (e.g., S, Cl, Br, Rb and Cs) the correlation is fairly strong and the C_X^{fluid} / C_X^{melt} ratios are almost independent of the absolute element concentration in the melt. It can be supposed that if the gas/melt elemental ratio does not depend on the absolute element concentration in the gas/melt system, then this ratio is under the control of equilibrium element partitioning (McIntire, 1963):

$$C_X^{fl} = K_d^{fl/melt} \times C_X^m \qquad (12).$$

The correlations C_X^{fluid} *vs.* C_X^{melt} for other elements are weakened by additional factors. In particular, deviation from the proportionality is possibly caused by systematic differences in $K_d^{*fl/melt}$ for some elements at different tectonic settings. The difference in $K_d^{fl/melt}$ between arc and rift/hotspot volcanoes is obvious for Na, K, Cu, Cd, Se, Te, Re, Tl and Bi. Copper, thallium and bismuth clearly prefer island-arc gases, while cadmium, selenium, tellurium and rhenium substantially enrich rift/hotspot gases. Concentrations of the listed elements in arc and rift/hotspot gases can differ by an order of magnitude, while concentrations of these elements in the corresponding melts are almost the same (Fig. 6). Elements

such as Al, Fe, Mn, V, Co and Th (low-volatility, predominantly aerosol-borne elements) have a narrow range of contents in the rocks simultaneously with a wide range of concentrations in gases (Fig. 5). Such behavior of low-volatility elements may be caused, in our opinion, by a large data scatter due to analytical uncertainties and errors caused by the subtraction of aerosol fraction from the measured values, as well as by fluctuations in the gas of elements transported predominantly as aerosols (e.g., Zelenski et al., 2014).

5.2. Partition coefficients in the volcanic gas – silicate melt system

To obtain values for *Kd*, we compared the weight concentrations of elements in gas and rock separately for each of the six selected volcanoes: $Kd \approx Kd^* = C_X^{fl} / C_X^{melt}$. The partition coefficients calculated for each of the elements and for each of the volcano are given in Annex 2, Supplementary Table S3. For most of the elements, the values of *Kd** calculated for different volcanoes do not coincide exactly, but fall within a certain range. Considering the problems with the data quality on trace element composition of volcanic gas (Section 4.1. and Annex 2), variations of the inferred Kd values ± a half-order of magnitude were regarded as good, and those ± one order of magnitude were regarded as satisfactory. Arc and rift/hotspot volcanoes were considered separately.

The most correct way to average the values with such large ranges is the geometric mean, which would be equidistant from both the maximum and minimum values of the parameter. The geometric mean suppresses the influence of very high or very low values. In the logarithmic scale, the logarithm of the geometric mean is equal to the arithmetic mean of the logarithms of the initial values. Partition coefficients averaged in such a way are given in Tables 5a and 4b separately for arc and rift/hotspot volcanoes and are shown on the diagram in the descending order, together with uncertainties (Fig. 7). The elements in Tables 5a, b are arranged in the order of decreasing Kd in the gases of island-arc volcanoes. If several values were determined for different volcanoes, then the average value and range are given. Elements with lower uncertainties (± half an order of magnitude) for the calculated Kd are shown in Table 5a, elements with high uncertainties are shown in Table 5b. If the *Kd** for an element was determined only for a single volcano, this value is also placed in Table 5b. Two exceptions were made for Os and Ir, which, due to their importance (platinum group elements and among the rarest elements on Earth), were placed in Table 5a.

Only 14 elements of 58 in Table 5 have average *Kd** >1. Expectedly, these are highly volatile elements (halogens, S, Se, and Te) as well as Re, Tl, Bi, Os, Cd, Au, In, and As. The calculated partition coefficients of all other elements are in the range of 0.5–0.0001, which indicates that the weight concentrations of these elements in volcanic gas are 2–10000 times lower than the concentrations in silicate melt. We did not include in our calculations REE and some other low-volatility elements due to generally low data quality on the abundances for these elements in volcanic gases. The two most

abundant metals in the gas, sodium and potassium, have only moderate Kd* values of 0.01–0.025 for arc gases and even lower for rift/hotspot gases. Kd for all other rock-forming elements are lower than 0.001.

A large partition coefficient does not necessarily mean a high concentration of an element in the gas. For example, the Kd* for rhenium exceeds 40 in the gases of the Kilauea volcano; however, in terms of the absolute concentration in the gas (0.05 ppm), this element is one of the rarest. On the contrary, potassium and sodium, which are two of the most common metals in volcanic gases, have relatively small partition coefficients of 0.01–0.03. Due to the fact that these elements are abundant in the melt, they are also abundant in the gas.

6. Discussion

6.1. Comparison with the previous data

To our knowledge, no detailed studies are available so far on trace element partitioning in the volcanic gas – silicate melt system. However, the ratios C_{fl}/C_m are present in several studies for a number of active volcanoes, including Kudryavy (Pokrovski et al., 2013) and Tolbachik (Zelenski et al., 2014). These authors did not discuss the question about how diffusion fractionation changes the measured C_{fl}/C_m ratios. Mather (2015) made a similar assessment for Etna and Masaya, although gas–melt partition coefficients were referred to as "volatility coefficients". Similarly to Pokrovski et al. (2013) and Zelenski et al., 2014, Mather (2015) did not include diffusion fractionation in her calculations, although she cited works by Mackenzie and Canil (2008) and Johnson and Canil (2011), who experimentally studied diffusion fractionation during the degassing of basaltic melt.

The fractionation of sulfur and halogens between melts and fluids was examined in many studies, but little attention has been paid to fractionation at atmospheric pressure. An exception is a study by Alletti et al. (2009), where they provided an equation for chlorine partitioning for a wide range of pressures:

$$Kd_{Cl}^{fl/m} = 12.732 \times P^{-0.0853} \quad (13)$$

where P is in MPa. According to Eqn. (13), the partition coefficient for chlorine is equal to 15.7 for the 2013 Tolbachik eruption (continental arc, basaltic trachyandesite). This value is 2.6 times less than was calculated herein for Tolbachik based on gas and rock data ($Kd_{Cl}^{fl/m} = 41.6$). Eqn. (13) is based on data with significant dispersion. Earlier, Iwasaki and Katsura (1967) experimentally investigated the dependence of the solubility of HCl in a basaltic melt in an atmosphere of pure HCl at pressures from 0.001 to 0.1 MPa. They obtained the dependence for basalt, whose composition is close to Tolbachik basalt, for a temperature of 1290 ° C:

$$\log C_{HCl} = 0.63 \times \log P_{HCl} - 0.583 \quad (14).$$

Substituting in Eqn. (14) data for the 2013 Tolbachik eruption (total P = 0.085 MPa, C_{HCl}^{fl} = 1.37 mol. % or 2.47 wt. % provides $Kd_{Cl}^{fl/m}$ for Tolbachik equal to 38.6, which is close to the calculated value of 41.6.

The partitioning of sulfur is more complex because it strongly depends on fO_2 (e.g., Moretti et al., 2003; Witham et al., 2012, and references therein). Although surficial degassing of basalt occurs in atmosphere containing ~20 % O_2, the fO_2 in rising bubbles is buffered by the melt before the bubbles reach the surface (more precisely, by the FeO/Fe_2O_3 ratio of the melt, Gerlach, 1993). We used data from Moretti et al. (2003) for the H–C–O–S fluid system to calculate the $Kd_S^{f/m}$ for Kilauea and Tolbachik volcanoes at different oxygen fugacities. For Kilauea lavas with fO_2 = NNO–0.5 (Gerlach, 1993), calculations using the model from Moretti at al. (2003) provided $Kd_S^{f/m}$ = 1863, which is higher than the $Kd_S^{fl/m}$ = 1044 calculated using the model proposed in this study. The discrepancy may arise either from a low estimate of fO_2 for Kilauea basalt or from too high concentration sulfur, assumed for melt. If we use, for our model sulfur content, a BHVO-1 of 102 ppm S rather than 180 ppm from the quenched melt spatter, then the obtained $Kd_S^{f/m}$ is 1843, which almost coincides with $Kd_S^{fl/m}$ = 1863 as calculated from the Moretti et al. (2003) model.

No data on fO_2 exists for lavas from the 2013 Tolbachik eruption, so we assessed fO_2 = NNO+1.65±0.55 for average Tolbachik basalts using ferric and ferrous concentrations in bulk rock analyses (Sack et al., 1980). At such fO_2, $Kd_S^{fl/m}$ is equal to 280, which is half that observed at 560. On the other hand, fO_2 for the 1941 Tolbachik magnesian basalt was calculated as equal to QFM+1.1 ~NNO+0.3 using the olivine-spinel pair (Kamenetsky et al., 2017). This oxygen fugacity corresponds to $Kd_S^{fl/m}$ = 1044, i.e., almost twice as high as observed. Seemingly, fO_2 for the 2013 Tolbachik basalt was somewhat higher than NNO+0.3, but lower than NNO+1.65; the observed $Kd_S^{f/m}$ = 560 corresponds to NNO+0.9. The considerations above show that the more precise data was used, the more calculated partition coefficients correspond to the observed values.

6.2. Partition coefficients at arc and rift/hotspot volcanoes

Trace-element compositions of volcanic gases on arc and rift/hotspot volcanoes are different. This was reported, for example, by Edmonds et al. (2018): “Explaining the systematic differences in trace-metal emissions between these arc and hotspot volcanoes requires consideration of the processes that partition metals during magma ascent and eruption”. These authors suggested that partitioning between silicate melt, aqueous fluid, and sulfide melt at a great depth as well as the timing of sulfide and brine

unmixing determines the metal endowment of surficial volcanic gases. Namely, if sulfides are separated from the melt before the aqueous fluid, then the chalcophile metals partition into the sulfide melt and do not reach the surface. Conversely, if an aqueous fluid phase forms before sulfide saturation and the sulfide saturation level of the melt is never reached, then the aqueous fluid will remain metal-rich and will be outgassed during magma ascent and eruption. Since sulfide saturation is strongly controlled by the fO_2 of the melt, and separation of the aqueous fluid depends on the initial water content, than these two factors have profound effect on metal endowment in the melt and in the gas when they reach the surface.

In the present article we propose a different hypothesis, suggesting that the trace-element composition of volcanic gases is almost solely determined by the near-surface partitioning of elements in the volcanic gas – silicate melt system. Deep processes only indirectly affect the composition of surficial gases through changing the composition of the silicate melt and concentrations of the main gas components. Rising fluid bubbles do not inherit the deep fluid composition, and after a short transient period, acquire the same metal contents as bubbles that nucleated and grew in the near-surface conditions (see Sections 3.3., 3.4., 6.4., and Annex 1). This statement is valid only for gas bubbles not exceeding several mm in diameter; otherwise the bubbles may not have time to fully equilibrate with the melt and their composition may maintain features of the deep fluid.

Below we show that the concentrations of major gas components (SO_2, H_2S, and HCl) is an important factor controlling the element partitioning in a surficial volcanic gas – silicate melt system. Elements in volcanic gas are transported in forms of various chemical compounds. The speciation of elements in volcanic gases is known from thermodynamic modeling and depends both on the elemental properties and on the relative abundances of main ligand-forming components (sulfur species and halides). Commonly, elements form small di- and triatomic molecules (halides, sulfides, hydrides, and oxides), and less often, more complex molecules (hydroxides). Some elements may exist as free atoms.

Using thermodynamic models from Symonds et al. (1992), Symonds and Reed (1993), Wahrenberger (1997), Churakov et al. (2000), Taran et al. (2001), and Pokrovski et al. (2002), we compiled a list of the main element species in volcanic gases for the temperature range of 800-1000 °C (Table 6). The listed species represent more than 99% in total of each element in the gas. The predominant gaseous species are compared with the calculated partition coefficients of the elements for the gas–melt systems of arc and rift/hotspot volcanoes. Elements in Table 6 are arranged in the order of decreasing difference between *Kd** calculated for arc gases and *Kd** calculated for rift/hotspot gases: $\Delta = \log(Kd^{arc}) - \log(Kd^{rift/hotspot})$. The thermodynamic modeling in the cited articles was performed for the pressure 1 bar, and the element speciation listed in Table 6 is only valid for the surface and near-surface conditions.

Table 6 demonstrates that all elements that prefer forming halides in the gas, such as alkali metals, V, Cr, Mn, Fe, Co, Cu, Ag, In, W, Tl and Bi have higher partition coefficients for the studied arc

volcanoes, where gases are enriched in HCl (average S/Cl molar ratio ~3.0, Fig. 2). Conversely, elements that preferably form hydrides, sulfides or free atoms, such as Zn, As, Se, Pb, Cd, and Te, demonstrate an affinity to rift/hotspot gases that are enriched in sulfur (average S/Cl molar ratio ~48 for the studied volcanoes, Fig. 2) and contain more reducing species, such as H_2 (mainly due to the gas buffer reaction $H_2S + 2H_2O = 3H_2 + SO_2$, Giggenbach, 1987) and CO. The list of elements that form sulfides or free atoms in a gas also includes Zn and Pb, although they also tend to form chlorides. Two exceptions are gold and molybdenum, which have a small difference of *Kd** between arc and rift/hotspot volcanoes.

As can be concluded from the above, the S/HCl ratio in the gas and element properties are two major factors affecting element partitioning in the surficial gas–melt system. The amount of water in the melt is another important factor. It follows from the Eqn. 5 and Eqn. 7 that the lower the H_2O content of the melt, the closer the gas–melt system approaches to equilibrium. Water content may have a significant effect on elements with high partition coefficients, such as Te, Se, and Re. Namely, low water content that is typical for rift/hotspot volcanoes, contributes attaining the equilibrium and increasing the observed partition coefficients for these elements (Table 5a).

6.3 Relations between partition coefficient (*Kd*) and enrichment factor (EF)

The enrichment factor (EF) is a concentration of an element of interest, normalized to the concentration of the same element in a rock and, in addition, to the conservative (typically non-volatile) reference element in a rock (Lepel et al., 1978; Zoller et al., 1983):

$$EF = \frac{(C_X / C_R)_{gas}}{(C_X / C_R)_{rock}} \qquad (15).$$

Here C_R stands for the concentration of a non-volatile reference element and C_X is the concentration of an element of interest; magma of known composition is supposed to form aerosol particles. From comparing Eqns. 11 and 15, one can find that they are connected by a simple ratio WAF = 1/EF. Aiuppa et al. (2003) also used the notation expressed in %. The concept of the WAF is more evident as it directly characterizes the contribution of the silicate aerosol fraction to the concentration of an element in a gas sample.

Enrichment factors are widely used in the environmental sciences to speculate on the origin of elements, if at least two different sources of the elements exist, one of which is a conservative source such as rock dust (Reimann and de Caritat, 2000). In the case of volcanic degassing, the use of EF yields especially good results, because it allows the separation of the silicate aerosol fraction and the fraction of elements that have left the melt in the form of volatile compounds.

The value of the EF varies from unity for the reference element to large values of the order of 10^6–10^7 for S, Se and Te and 10^4–10^6 for some chalcophile and highly siderophile elements. This creates the

impression that these elements have high partition coefficients in the gas–melt system. In fact, this is not the case. From $Kd \approx \frac{C_X^{gas}}{C_X^{melt}}$, by a simple conversion, we obtain

$$EF \approx Kd \times \frac{(C_R)_{melt}}{(C_R)_{gas}} \quad (16).$$

Eqn. (16) is correct only for raw gas analyses, i.e., for those analyses that were not "purified" from the silicate aerosol using the EF procedure. Typically, the ratio $\frac{(C_R)_{melt}}{(C_R)_{gas}}$ is in the range of 10^3–10^5 and depends on the arbitrary choice of the reference element and on a random factor, such as the concentration of silicate aerosol in the gas condensate or aerosol sample. For example, for the present article, we used ytterbium as a reference element, in which case the $\frac{(C_{Yb})_{melt}}{(C_{Yb})_{gas}}$ ratio equals to ~21,000 on average for Tolbachik gas and $log\left(\frac{(C_{Yb})_{melt}}{(C_{Yb})_{gas}}\right) \approx 4.322$. Thus, the typical EF values in the volcanic gas - silicate melt system are 10^4-–10^5 times higher than the calculated mass partition coefficients *Kd** and depend randomly on the concentration of silicate aerosol in the samples (Fig. 8).

6.4 Relation between deep magmatic fluid and volcanic gas

In response to decompression, the fluid in bubbles exsolved from a rising melt gradually changes its composition from CO_2-rich to H_2O-rich, and then ,with the pressure decreasing, sulfur and chlorine compounds (and thus their volatile compounds) become increasingly important (e.g., Newman and Lowenstern, 2002, Witham et al., 2012, and references therein). It has long been known that the temperature and pressure dependence of the standard reaction properties for homogeneous and heterogeneous equilibria can be successfully described by the density model, which is based on the log-log linear relationship between the logarithm of the equilibrium constant and the logarithm of the H_2O density. This tool is applicable to association-dissociation equilibria and solid phase solubilities over a wide range of solvent densities, that is, from the low-pressure aqueous vapor to high-pressure fluids (Franck 1956; Marshall and Franck 1981, see also the review by Dolejš (2013). Pokrovski et al. (2005, 2013) confirmed this for the aqueous "liquid - vapor" system. Currently, there is no available data on the gas-melt partitioning for the magmatic vapor - silicate melt system at elevated pressures. We think however, that the linear log-log dependence of metal concentrations vs. the gas density (with a constant gas composition) may be also valid for such a system. In other words, Kd depends not only on the fluid composition, but also on the fluid density.

Changes in the concentration of ligand-forming components (HCl, SO_2,and H_2S), and in particular, a sharp increase in HCl near the surface caused by a preferential partition of HCl in the gas at low pressures (Iwasaki and Katsura, 1967; Aletti et al., 2009; Shinohara, 2009; Witham et al., 2012), significantly affect the speciation of metals (see Table 6 and references cited in Section 6.2), and, therefore, the partial pressures of the corresponding element species. As the density and composition of the fluid in terms of major gas species evolve during decompression, the concentrations of trace elements metals in the fluid change in a complex way and are extremely difficult to calculate.

A lava flow have no connection with deep magma, whereas a stable gas flux from a lava lake is supported by magma convection (e.g., a review from Pering et al., 2019), which carries deep fluid bubbles to the surface. The question arises of how fast the rising bubbles equilibrate their element content with the surrounding melt during the bubble ascent. If equilibration at every point of the bubble ascent takes place, then gas emissions from lava lakes should be similar to that from lava flows. If rising bubbles inherit trace element contents of deep dense fluid, then the partition coefficients measured on lava lakes and open-vent volcanoes should be higher than those measured at surficial lava flows.

We showed (Section 3.4.), that for small bubbles with the diameter ≤1 mm, equilibration may be attained sufficiently fast. However, the equilibration rate of rising bubbles decreases inversely with the square of their diameter, and for large bubbles may not be fast enough to attain equilibrium with the melt in respect to many elements. To answer whether the equilibration between the rising bubbles and the silicate melt takes place beneath the surface of convecting magma, we compared, side by side, the partition coefficients observed for a lava flow (the 2013 Tolbachik eruption) and for open-vent volcanoes Ambrym, Masaya and Etna (Fig. 9). In order to eliminate the influence of the different gas composition for arc and rift/hotspot volcanoes, only arc volcanoes were taken for the comparison. The graph in Fig. 9 demonstrates that most Kd^{vent} / Kd^{flow} ratios are close to unity (0.5 - 2), including volatile elements (S, F, Cl, and Br) that are close to the 1:1 line. Only a few points have a ratio of approximately 3. Index “vent” stands here for convective degassing (open-vent volcanoes with convective mass exchange with deep magma), and “*fl*ow” designates non-convective degassing of a lava flow. The comparison in Fig. 9 shows that the trace-element composition of the volcanic gas released from open-vent volcanoes with convecting magma (Ambrym, Masaya, Etna) is almost completely determined by the near-surface gas–melt partitioning.

6.5. Implications

Information about element partitioning in the volcanic gas – silicate melt system may be important for studying the volcanic degassing, the influence of the volcanic emissions on the atmosphere and environment, and in an assessment of the global circulation of elements (e.g., Mather et al., 2003; Delmelle, 2003; Mather, 2015, and references therein). For example, knowing the melt composition and

the bulk emission of SO_2 during a major basaltic eruption, one can estimate the emissions for each of the trace elements for a volcano, where direct measurements of the trace-element composition are absent. However, the data on element partitioning during surficial degassing are applicable for estimating metal emissions only from non-explosive basaltic eruptions. Eruptions of andesitic volcanoes with a high explosivity index are driven by expansion of dense deep fluid bubbles (e.g., Sparks, 1978). The metal content, the partition coefficients in the dense fluid–melt system and the extent of the equilibration between fluid and melt during fast explosive decompression are generally unknown.

Another possible application of element partitioning in the volcanic gas – silicate melt system may be in the solution of so-called inverse problems. This can be illustrated as follows. We know what the volcanic system provides at the output point (fumarolic gas), and we want to find out what is happening inside the system (e.g., composition of the degassing magma). Many volcanoes have a complex structure and diverse rock compositions, so it is not known exactly what the composition of the degassing melt is. If we compare the element ratios in volcanic gases and in rocks, then we can make assumptions about the composition of the melt that is currently degassing. For example, Kudryavy volcano, Iturup, Kurile Island is a persistently degassing composite volcano (Taran et al., 1995; Wahrenberger, 1997) composed of different rocks from primitive basalts to andesites and even rhyodacites. All these rocks have distinctly different abundances of some incompatible and moderately volatile elements such as Na, K, and Pb (Yudovskaya et al., 2008; Martynov et al., 2010).

We calculated the gas composition, which theoretically could be exsolved from basalt, andesite, and rhyodacite from Kudryavy volcano according to Eqn. $C_X^{fl} = K_d^{fl/melt} \times C_X^m$ and compared the calculated values with the measured gas compositions. The calculated ratios K/Na = 0.69, K/Pb = 36, and Na/Pb = 52 for the degassing andesite from Kudryavy closely matched the analyses of the fumarole 870 °C (K/Na = 0.72, K/Pb = 48 and Na/Pb = 68, Taran et al. (1995), whereas the calculated compositions of gases from basalt and rhyodacite do not show any coincidence as well as with gases from all other fumaroles (Taran et al., 1995; Wahrenberger, 1997) did not show any coincidence. Certainly, such calculations provide only a rough approximation because they do not take the into account fractionation of fumarolic gas along its path from magma to the surface.

7. Conclusions

1. Surficial or near-surface degassing of basaltic melt, i.e., isobaric degassing at atmospheric pressure and small supersaturations in water, is a specific degassing mode with particular features. The increased expansion of low-density fluid bubbles results in thinning of the diffusion boundary layer around the growing bubble and, thereby, in the significant weakening of the diffusion fractionation of elements. As a result, the observed partition coefficients *Kd** measured in volcanic

gases are close to the equilibrium partition coefficients *Kd* in the volcanic gas – silicate melt system for the majority of elements, except for the most volatile trace elements, such as Se and Te.

2. Diffusion-driven bubble growth and ascent in approximately isobaric conditions is a major way of degassing for lava flows. Bubbles transported by the ascending magma to the surface rapidly re-equilibrate with the isobaric surficial melt. For elements with partition coefficients less than 0.01, the characteristic diffusion distance is on the order of 10 atomic layers or less (for 1- mm bubbles), which is an additional factor in the rapid re-equilibration of surface melt and fluid. The contribution of the degassing directly from the free melt surface is negligible.

3. The observed partition coefficients *Kd** in the near-surface volcanic gas – silicate melt system for the 58 studied elements range from 10^{-4} to 10^{3}, i.e., within seven orders of magnitude. For 14 elements, the observed *Kd** > 1, including volatile elements S, Se, Te, halogens, Tl, Re, Os, Bi, Cd, Au, In and As. Alkali metals have *Kd** in the range of 0.1 for Cs to 0.01 for Na. The observed *Kd** of the other rock-forming elements are < 0.001. The observed *Kd** values are correct to within half an order of magnitude. The existing dataset of volcanic rock and volcanic gas analyses does not allow for the calculation of *Kd** for low-volatility elements, such as REE and HFSE.

4. Less than a three-fold differences in *Kd** measured for open-vent volcanoes (connection exists with deep magma) and *Kd** for a lava flow (no connection with deep magma) indicates that that the trace element composition of surficial volcanic gases does not depend on the composition of deep fluid bubbles due to the rapid re-equilibration from the decompression – diffusion to the isobaric (diffusion-driven) growth modes.

5. The low water content, high sulfur to chlorine ratio in rift/hotspot magmas and high temperature of the melt are additional factors determining partition coefficients of elements in the gas – melt system. Another important factor is the element speciation in the gas. Elements that are transported in the gas predominantly as halides have higher partition coefficients in HCl-rich arc gases. Such elements that prefer to exist in the gas as sulfides, hydrides, and free atoms, demonstrate affinity to sulfur-rich, HCl-poor rift/hotspot gases. The observed increased concentrations in rift/hotspot gases of Re, Te, Se and Cd and vice versa, increased concentrations in arc gases of Cu, Bi, Na, K, appears largely due to the difference in partitioning of the listed elements depending on the gas composition and element speciation.

6. Data on the element partitioning in the volcanic gas – silicate melt system may be used in the assessment of global element emissions by volcanoes and in deciphering the composition of the magmatic source of persistently degassing volcanoes.

Acknowledgements

We would like to thank Nicole Hurtig, Jacob Lowenstern and an anonymous reviewer for their thoughtful comments, which allowed us to greatly improve the manuscript. This work was supported by RFBR grant #19-05-00777A. VSK thanks the Australian Research Council (DP200100406) for funding the research on gas/rock interaction.

References

Aiuppa, A., Dongarra, G., Valenza, M., Federico, C. and Pecoraino, G. (2003) Degassing of trace volatile metals during the 2001 eruption of Etna. In *Volcanism and the Earth's Atmosphere* (Eds. A. Robock and C. Oppenheimer). Geophysical Monograph Series **139**. pp. 41–54. American Geophysical Union, Washington, DC. https://doi.org/10.1029/139GM03

Aiuppa, A., Federico, C., Giudice, G., Gurrieri, S., Paonita, A. and Valenza, M. (2004) Plume chemistry provides insights into mechanisms of sulfur and halogen degassing in basaltic volcanoes. *Earth. Planet. Sci. Lett.* **222**, 469–483. https://doi.org/10.1016/j.epsl.2004.03.020

Allard, P., Aiuppa, A., Loyer, H., Carrot, F., Gaudry, A., Pinte, G., Michel, A. and Dongarrà, G. (2000) Acid gas and metal emission rates during long-lived basalt degassing at Stromboli volcano. *Geophys. Res. Lett.* **27**, 1207–1210. https://doi.org/10.1029/1999GL008413

Allard, P., Aiuppa, A., Bani, P., Metrich, N., Bertagnini, A., Gauthier, P. J., Shinohara, H., Sawyer, G., Parello, F., Bagnato, E., Pelletier, B. and Garaebiti, E. (2016). Prodigious emission rates and magma degassing budget of major, trace and radioactive volatile species from Ambrym basaltic volcano, Vanuatu island Arc. *J. Volcanol. Geotherm. Res*., **322**, 119–143. https://doi.org/10.1016/j.jvolgeores.2015.10.004

Alletti, M., Baker, D. R., Scaillet, B., Aiuppa, A., Moretti, R. and Ottolini, L. (2009) Chlorine partitioning between a basaltic melt and H_2O-CO_2 fluids at Mount Etna. *Chem. Geol.* **263**, 37-50. https://doi.org/10.1016/j.chemgeo.2009.04.003

Audétat, A., Günther, D. and Heinrich, C. A. (1998) Formation of a magmatic-hydrothermal ore deposit: Insights with LA-ICP- MS analysis of fluid inclusions. *Science* **279**, 2091–2094. https://doi.org/10.1126/science.279.5359.2091

Ault, W. U., Eaton J. P. and Richter, D. H. (1961) Lava temperatures in the 1959 Kilauea eruption and cooling lake. *Geol. Soc. Am. Bull.* **72**, 791 – 794. https://doi.org/10.1130/0016-7606(1961)72[791:LTITKE]2.0.CO;2

Baker, D. R. and Balcone-Boissard, H. (2009) Halogen diffusion in magmatic systems: Our current state of knowledge. *Chem. Geol.* **263**, 82–88. https://doi.org/10.1016/j.chemgeo.2008.10.010

Beattie, P., Drake, M., Jones, J., Leeman, W., Longhi, J., McKay, G., Nielsen, R., Palme, H., Shaw, D., Takahashi E., and Watson, B. (1993) Terminology for trace-element partitioning, *Geochim. Cosmochim. Acta* **57**, 1605–1606. https://doi.org/10.1016/0016-7037(93)90015-O

Beerkens, R. G. (2001) Modeling the Kinetics of Volatilization from Glass Melts. *J. Am. Ceramic Soc.,* **25**, 1952-1960.

Berthelot, M. (1872) On the law which governs the distribution of a substance between two solvents. *Ann. Chim. Phys. (4th series)* **26**, 408-417.

Bottinga, Y. and Javoy, M. (1991) The degassing of Hawaiian tholeiite. *Bull. Volcanol.* **53**, 73–85. https://doi.org/10.1007/BF00265413

Brady, J. B. (1995) Diffusion Data for Silicate Minerals, Glasses, and Liquids. In *Mineral Physics & Crystallography: A Handbook of Physical Constants, Vol. 2.* (Ed. T. J. Ahrens). AGU, Washington, DC. pp. 269–290 https://doi.org/10.1029/RF002

Cable, M. (1978) Kinetics of Volatilization of Sodium Borate Melts. In: Pye L.D., Fréchette V.D., Kreidl N.J. (Eds.) Borate Glasses. Materials Science Research, vol 12. Springer, Boston, MA. https://doi.org/10.1007/978-1-4684-3357-9_20

Cashman, K., Mangan, M. T., and Newman, S. (1994) Surface degassing and modifications to vesicle size distributions in active basalt flows. *J. Volcanol. Geotherm. Res*. **61**, 45–68. https://doi.org/10.1016/0377-0273(94)00015-8

Chanson H. (2004) Summary of basic hydraulic principles. In: Hydraulics of Open Channel Flow. An Introduction Basic Principles, Sediment Motion, Hydraulic Modelling, Design of Hydraulic Structures. 2nd Edition, Butterworth-Heinemann, 2004. https://doi.org/10.1016/B978-0-7506-5978-9.X5000-4

Chevrel, M. O., Harris, A. J. L., James, M. R., Calabrò, L., Gurioli, L. and Pinkerton, H. (2018) The viscosity of pāhoehoe lava: In situ syn-eruptive measurements from Kilauea, Hawaii. *Earth. Planet. Sci. Lett.* **493**, 161–171. https://doi.org/10.1016/j.epsl.2018.04.028

Churakov, S. V., Tkachenko, S. I., Korzhinskii, M., Bocharnikov, R. E. and Shmulovich, K. I. (2000) Evolution of composition of high-temperature fumarolic gases from Kudryavy Volcano, Iturup, Kuril Islands: the thermodynamic modeling. *Geochem. Int.* **38**, 436–451.

Crank, J. (1975) The Mathematics of Diffusion, 2nd edition, Oxford University Press, Oxford.

Crowe, B. M., Finnegan, D. L., Zoller, W. H. and Boynton, W. V. (1987) Trace element geochemistry of volcanic gases and particles from 1983–1984 eruptive episodes of Kilauea volcano. *J. Geophys. Res.* **92(B13)**, 13708–13714. https://doi.org/10.1029/JB092iB13p13708

Delmelle, P. (2003) Environmental impacts of tropospheric volcanic gas plumes. *Geological Society, London, Special Publications* **213**, 381-399. https://doi.org/10.1144/GSL.SP.2003.213.01.23

Dolejs, D. (2013) Thermodynamics of Aqueous Species at High Temperatures and Pressures: Equations of State and Transport Theory. Rev. Mineral. and Geochem.**76**, 35-79. doi:https://doi.org/10.2138/rmg.2013.76.3

Duffell, H. J., Oppenheimer, C., Pyle, D. M., Galle, B., McGonigle, A. J. S. and Burton, M. R. (2003) Changes in gas composition prior to a minor explosive eruption at Masaya volcano, Nicaragua. *J. Volcanol. Geotherm. Res.* **126**, 327–339. https://doi.org/10.1016/S0377-0273(03)00156-2

Edmonds, M., Mather, T. A. and Liu, E. J. (2018) A distinct metal fingerprint in arc volcanic emissions. *Nat. Geosci.* **11**, 790-794. https://doi.org/10.1038/s41561-018-0214-5

Fischer, T. P. and Chiodini, G. (2015) Volcanic, Magmatic and Hydrothermal Gases. In *The Encyclopedia of Volcanoes (2nd Edition)*. (eds. Sigurdsson, H., Houghton, B., McNutt, S., Rymer, H. and Stix, J.) Elsevier Inc. https://doi.org/10.1016/b978-0-12-385938-9.00045-6

Gaonac'h, H., Lovejoy, S., Stix, J. and Scherzter, D. (1996a) A scaling growth model for bubbles in basaltic lava flows. *Earth. Planet. Sci. Lett.* **139**, 395–409. https://doi.org/10.1016/0012-821X(96)00039-8

Gaonac'h, H., Stix, J. and Lovejoy, S. (1996b) Scaling effects on vesicle shape, size and heterogeneity of lavas from Mount Etna. *J. Volcanol. Geotherm. Res*. **74**, 131-153. https://doi.org/10.1016/S0377-0273(96)00045-5

Gauthier, P., Sigmarsson, O., Gouhier, M., Haddadi, B. and Moune, S. (2016) Elevated gas flux and trace metal degassing from the 2014–2015 fissure eruption at the Bárðarbunga volcanic system, Iceland. *J. Geophys. Res. Solid Earth* **121**, 1610–1630. https://doi.org/10.1002/2015JB012111

Gerlach, T. M. (1979) Evaluation and restoration of the 1970 volcanic gas analyses from Mount Etna, Sicily. *J. Volcanol. Geotherm. Res.* **6**, 165–178. https://doi.org/10.1016/0377-0273(79)90052-0

Gerlach, T. M. (1993) Oxygen buffering of Kilauea volcanic gases and the oxygen fugacity of Kilauea basalt. *Geochim. Cosmochim. Acta* **57**, 795–814. https://doi.org/10.1016/0016-7037(93)90169-W

Gerlach, T. M. and Graeber, E. J. (1985) Volatile budget of Kilauea volcano. *Nature* **313**, 273–277. https://doi.org/10.1038/313273a0

Giggenbach, W.F. and Le Guern, F., 1976. The chemistry of magmatic gases from Erta'Ale, Ethiopia. *Geochim. Cosmochim. Acta* **40**, 25–30. https://doi.org/10.1016/0016-7037(76)90190-3

Giggenbach, W. F. (1987) Redox processes governing the chemistry of fumarolic gas discharges from White Island, New Zealand. *J. Appl. Geochem.* **2**, 143–161. https://doi.org/10.1016/0883-2927(87)90030-8

Giordano, D., Russell, J. K. and Dingwell, D. B. (2008) Viscosity of magmatic liquids: A model. *Earth. Planet. Sci. Lett.* **271**, 123–134. https://doi.org/10.1016/j.epsl.2008.03.038

Gladney, E. S. and Roelandts, I. (1988) 1987 compilation of elemental concentration data for USGS BHVO-1, MAG-1, QLO-1, RGM-1, SCo-1, SDC-1, SGR-1, and STM-1. Geostand. Geoanal. Res. 12, 253–362. https://doi.org/10.1111/j.1751-908X.1988.tb00053.x

Greenland, L. P. (1984) Gas composition of the January 1983 eruption of Kilauea Volcano, Hawaii. *Geochim. Cosmochim. Acta* **48**, 193–195. https://doi.org/10.1016/0016-7037(84)90361-2

Hedenquist J.W. (1995) The ascent of magmatic fluids: Eruption versus mineralization. In *Magmas, Fluids and Ore Deposits* (ed. Thompson J. F.), Short Course 23, Mineralogical Association of Canada, Victoria, Canada. pp. 263-289.

Henley, R. W. and Berger, B. R. (2013) Nature's refineries - Metals and metalloids in arc volcanoes. *Earth-Sci. Rev.* **125**, 146–170. https://doi.org/10.1016/j.earscirev.2013.07.007

Hinkley, T. K., Lamothe, P. J., Wilson, S. A., Finnegan, D. L. and Gerlach, T. M. (1999) Metal emissions from Kilauea, and a suggested revision of the estimated worldwide metal output by quiescent degassing of volcanoes. *Earth. Planet. Sci. Lett.* **170**, 315–325. https://doi.org/10.1016/S0012-821X(99)00103-X

Iwasaki, B. and Katsura, T. (1967) The Solubility of Hydrogen Chloride in Volcanic Rock Melts at a Total Pressure of One Atmosphere and at Temperatures of 1200°C and 1290°C under Anhydrous Conditions. Bull. *Chem. Soc. Japan* **40**, 554-561. https://doi.org/10.1246/bcsj.40.554

Johnson, A. and Canil, D. (2011) The degassing behavior of Au, Tl, As, Pb, Re, Cd and Bi from silicate liquids: Experiments and applications. *Geochim. Cosmochim. Acta* **75**, 1773–1784. https://doi.org/10.1016/j.gca.2010.12.023

Kamenetsky, V. S., Zelenski, M., Gurenko, A. A., Portnyagin, M. V., Ehrig, K., Kamenetsky, M., Churikova, T. and Feig, S. (2017) Silicate-sulfide liquid immiscibility in modern arc basalt (Tolbachik volcano, Kamchatka): Part II. Composition, liquidus assemblage and fractionation of the silicate melt. *Chem. Geol*. **471**, 92-110. https://doi.org/10.1016/j.chemgeo.2017.09.019

Lamb, H. (1932) Hydrodynamics, 6th ed., 738 pp., Dover, Mineola, N.Y.

Lambert, G., Le Cloarec, M. F., Ardouin, B. and Le Roulley, J. C. (1985) Volcanic emission of radionuclides and magma dynamics. *Earth. Planet. Sci. Lett*., **76**, 185–192. https://doi.org/10.1016/0012-821X(85)90158-X

Lassiter, J. C. (2003). Rhenium volatility in subaerial lavas: constraints from subaerial and submarine portions of the HSDP-2 Mauna Kea drillcore. Earth Planet. Sci. Lett. 214, 311-325. https://doi.org/10.1016/S0012-821X(03)00385-6

Lenoir, M., Neuville, D. R., Malki, M., Grandjjean, A. (2010). Volatilization kinetics of sulphur from borosilicate melts: A correlation between sulphur diffusion and melt viscosity. J. Non-Cryst. Solids, 356, 2722–2727. https://doi.org/10.1016/j.jnoncrysol.2010.09.077

Lepel, E. A., Stefansson, K. M. and Zoller, W. H. (1978) The enrichment of volatile elements in the atmosphere by volcanic activity: Augustine Volcano 1976. J. Geophys. Res. 83, 6213–6220. https://doi.org/10.1029/JC083iC12p06213

Van Limpt, H., Beerkens, R., Cook, S., O'Connor, R. and Simon, J. (2011). Modelling the evaporation of boron species. Part 1. Alkali-free borosilicate glass melts. Glass Technology: European Journal of Glass Science and Technology Part A, **52**, 77–87.

MacKenzie, J. M. and Canil, D. (2008) Volatile heavy metal mobility in silicate liquids: Implications for volcanic degassing and eruption prediction. *Earth. Planet. Sci. Lett*. **269**, 488–495. https://doi.org/10.1016/j.epsl.2008.03.005

Mangan, M. T., Cashman, K. V. and Newman, S. (1993) Vesiculation of basaltic magma during eruption. *Geology*, 21, 157–160. https://doi.org/10.1130/0091-7613(1993)021<0157:VOBMDE>2.3.CO;2

Martin, R. S., Sawyer, G. M., Day, J. A., Le Blond, J. S., Ilyinskaya, E. and Oppenheimer, C. (2012) High-resolution size distributions and emission fluxes of trace elements from Masaya volcano, Nicaragua. *J. Geophys. Res*. **117(B8)**, 1–12. https://doi.org/10.1029/2012JB009487

Martynov, Yu. A., Khanchuk, A. Kimura, J.-I., Rybin A. V. and Martynov A. Yu. (2010) Geochemistry and Petrogenesis of Volcanic Rocks in the Kuril Island Arc. *Petrology* **18**, 489-513. https://doi.org/10.1134/S0869591110050048

Mather, T. A., Pyle, D. M. and Oppenheimer, C. (2003) Tropospheric volcanic aerosol. In *Volcanism and the Earth's Atmosphere* (Eds. A. Robock and C. Oppenheimer). Geophysical Monograph Series **139**. American Geophysical Union, Washington, DC. pp. 189-212. https://doi.org/10.1029/139GM12

Mather, T. A. (2015) Volcanoes and the environment: Lessons for understanding Earth's past and future from studies of present-day volcanic emissions. *J. Volcanol. Geotherm. Res*. **304**, 160–179. https://doi.org/10.1016/j.jvolgeores.2015.08.016

Mather, T. A., Witt, M. L. I., Pyle, D. M., Quayle, B. M., Aiuppa, A., Bagnato, E., Martin, R.S., Sims, K. W. W., Edmonds, M., Sutton A. J. and Ilyinskaya, E. (2012) Halogens and trace metal emissions from the ongoing 2008 summit eruption of Kīlauea volcano, Hawai`i. *Geochim. Cosmochim. Acta* **83**, 292–323. https://doi.org/10.1016/j.gca.2011.11.029

McIntire, W. L. (1963) Trace element partition coefficients—a review of theory and applications to geology. *Geochim. Cosmochim. Acta* **27**, 1209–1264. https://doi.org/10.1016/0016-7037(63)90049-8

Moretti, R. Papale P. and Ottonello G. (2003) A model for the saturation of C-O-H-S fluids in silicate melts. *Geological Society, London, Special Publications* **213**, 81-101. https://doi.org/10.1144/GSL.SP.2003.213.01.06

Nernst, W. (1891) Distribution of a substance between two solvents and between solvent and vapor. *Z. Phys. Chem.* **8**, 110-139.

Newman, S. and Lowenstern, J. B. (2002). VolatileCalc: a silicate melt–H_2O–CO_2 solution model written in Visual Basic for excel. *Comput. Geosci-UK* **28**, 597–604. https://doi.org/10.1016/S0098-3004(01)00081-4

Ni, H. and Zhang, L. (2018) A general model of water diffusivity in calc-alkaline silicate melts and glasses. *Chem. Geol.* **478**, 60-68. https://doi.org/10.1016/j.chemgeo.2017.10.010

Nriagu, J. O. (1989) A global assessment of natural sources of atmospheric trace metals. *Nature* **338**, 47–49. https://doi.org/10.1038/338047a0

Olmez, I., Finnegan, D. L. and Zoller, W. H. (1986) Iridium emissions from Kilauea volcano. *J. Geophys. Res.* **91**, 653–663. https://doi.org/10.1029/JB091iB01p00653

Pennisi, M., Le Cloarec, M. F., Lambert, G. and Le Roulley, J. C. (1988). Fractionation of metals in volcanic emissions. *Earth. Planet. Sci. Lett*., **88**, 284–288. https://doi.org/10.1016/0012-821X(88)90085-4

Pering, T. D., Ilanko, T., Wilkes, T. C., England, R. A., Silcock, S. R., Stanger, L. R., Willmott, J. R., Bryant, R. G. and McGonigle A. J. S. (2019). A rapidly convecting Lava Lake at Masaya Volcano, Nicaragua. Front. Earth Sci. **6**, 241. https://doi.org/10.3389/feart.2018.00241

Plechov, P. Y., Blundy, J. D., Nekrylov, N., Melekhova, E., Shcherbakov, V. D. and Tikhonova, M. S. (2015) Petrology and volatile content of magmas erupted from Tolbachik Volcano, Kamchatka, 2012-13. J. Volcanol. Geotherm. Res. **307**, 182–199. https://doi.org/10.1016/j.jvolgeores.2015.08.011

Pokrovski, G. S., Zakirov, I. V., Roux, J., Testemale, D., Hazemann, J.-L., Bychkov, A. Y. and Golikova, G. V. (2002) Experimental study of arsenic speciation in vapor phase to 500°C: Implications for As transport and fractionation in low-density crustal fluids and volcanic gases. *Geochim. Cosmochim. Acta* **66**, 3453–3480. https://doi.org/10.1016/S0016-7037(02)00946-8

Pokrovski, G. S., Roux, J. and Harrichoury, J.-C. (2005) Fluid density control on vapor-liquid partitioning of metals in hydrothermal systems. *Geology*, **33**, 657. https://doi.org/10.1130/G21475.1

Pokrovski, G. S., Borisova, A. Y. and Bychkov, A. Y. (2013) Speciation and Transport of Metals and Metalloids in Geological Vapors. In *Reviews in Mineralogy and Geochemistry* **76** *(eds.* Stefánsson, A., Driesner, T. and Bénézeth, P.). Mineralogical Society of America, Washington, DC. pp. 165–218. https://doi.org/10.2138/rmg.2013.76.6

Reimann, C. and de Caritat, P. (2000) Intrinsic Flaws of Element Enrichment Factors (EFs) in Environmental Geochemistry. Environ. Sci. Technol. 34, 5084-5091. https://doi.org/10.1021/es001339o

Sack, R. O., Carmichael, I. S. E., Rivers, M. and Ghiorso, M. S. (1980) Ferric-ferrous equilibria in natural silicate liquids at 1 bar. *Contrib. Mineral. Petrol.* **75**, 369–376. https://doi.org/10.1007/BF00374720

Shinohara, H. (2009). A missing link between volcanic degassing and experimental studies on chloride partitioning. Chem.l Geology, 263(1–4), 51–59. https://doi.org/10.1016/j.chemgeo.2008.12.001

Shinohara, H., Aiuppa, A., Giudice, G., Gurrieri, S. and Liuzzo, M. (2008) Variation of H_2O/CO_2 and CO_2/SO_2 ratios of volcanic gases discharged by continuous degassing of Mount Etna volcano, Italy. *J. Geophys. Res.* **113(B9)**, B09203. https://doi.org/10.1029/2007JB005185

Sparks, R. S. J. (1978) The dynamics of bubble formation and growth in magmas: A review and analysis. *Phys. Earth and Planet. Int.* **13**, 161. https://doi.org/10.1016/0031-9201(76)90082-0

Stolper, E. (1982) The speciation of water in silicate melts. *Geochim. Cosmochim. Acta* **46**, 2609–2620. https://doi.org/10.1016/0016-7037(82)90381-7

Symonds, R. B. and Reed, M. H. (1993) Calculation of multicomponent chemical equilibria in gas-solid-liquid systems: calculation methods, thermochemical data, and applications to studies of high-temperature volcanic gases with examples from Mount St. Helens. *Am. J. Sci.* **293**, 758–864. https://doi.org/10.2475/ajs.293.8.758

Symonds, R. B., Reed, M. H. and Rose, W. I. (1992) Origin, speciation, and fluxes of trace-element gases at Augustine volcano, Alaska: Insights into magma degassing and fumarolic processes. *Geochim. Cosmochim. Acta* **56**, 633–657. https://doi.org/10.1016/0016-7037(92)90087-Y

Symonds, R. B., Rose, W. I., Bluth, G. J. S. and Gerlach, T. M. (1994) Volcanic gas studies: methods, results and applications. In: Volatiles in Magmas. (Eds. Carroll, M.R. and Hollaway, J.R.). *Reviews in Mineralogy and Geochemistry,* **30**, Mineralogical Society of America, Washington D.C. pp. 1-66.

Taran, Y. A., Hedenquist, J. W., Korzhinskii, M., Tkachenko, S. I. and Shmulovich, K. I. (1995) Geochemistry of magmatic gases from Kudryavy volcano, Iturup, Kuril Islands. *Geochim. Cosmochim. Acta* **59**, 1749–1761. https://doi.org/10.1016/0016-7037(95)00079-F

Taran, Y. A., Bernard, A., Gavilanes, J.-C., Lunezheva, E., Cortes, A. and Armienta, M. A. (2001) Chemistry and mineralogy of high-temperature gas discharges from Colima volcano, Mexico. Implications for magmatic gas–atmosphere interaction. *J. Volcanol. Geotherm. Res.* **108**, 245–264. https://doi.org/10.1016/S0377-0273(00)00289-4

Verma, S. P., Rosales-Rivera, M., Díaz-González, L. and Quiroz-Ruiz, A. (2017). Improved composition of hawaiian basalt BHVO-1 from the application of two new and three conventional recursive discordancy tests. Turk. J. Earth Sci. 26(5), 331–353. https://doi.org/10.3906/yer-1703-16

Wahrenberger, C. M. (1997) Some aspects of the chemistry of volcanic gases. Ph.D. Thesis. Zurich.

Wallace, P. J. and Anderson, A. T. (1998) Effects of eruption and lava drainback on the H_2O contents of basaltic magmas at Kilauea Volcano. *Bull. Volcanol*. **59**, 327–344. https://doi.org/10.1007/s004450050195

Watson, E. B. (2017) Diffusive fractionation of volatiles and their isotopes during bubble growth in magmas. *Contrib. Mineral. Petrol.* **172**, 1–21. https://doi.org/10.1007/s00410-017-1384-7

Witham, F., Blundy, J. D., Kohn, S. C., Lesne, P., Dixon, J. E., Churakov, S. V. and Botcharnikov, R. E. (2012) SolEx: A model for mixed COHSCl-volatile solubilities and exsolved gas compositions in basalt. *Comput. Geosci-UK* **45**, 87–97. https://doi.org/10.1016/j.cageo.2011.09.021

Yudovskaya, M. A., Tessalina, S. Distler, V. V. Chaplygin, I. V. Chugaev, A. V. Dikov, Y. P. (2008) Behavior of highly-siderophile elements during magma degassing: A case study at the Kudryavy volcano. *Chem. Geol*. **248**, 318-341. https://doi.org/10.1016/j.chemgeo.2007.12.008

Zelenski, M., Fischer, T. P., de Moor, J. M., Marty, B., Zimmermann, L., Ayalew, D., Nekrasov, A. N. and Karandashev, V. K. (2013) Trace elements in the gas emissions from the Erta Ale volcano, Afar, Ethiopia. *Chem. Geol.* **357**, 95–116. https://doi.org/10.1016/j.chemgeo.2013.08.022

Zelenski, M., Malik, N. and Taran, Y. A. (2014). Emissions of trace elements during the 2012–2013 effusive eruption of Tolbachik volcano, Kamchatka: enrichment factors, partition coefficients and aerosol contribution. *J. Volcanol. Geotherm. Res*. **285**, 136–149. https://doi.org/10.1016/j.jvolgeores.2014.08.007

Zhang, Y. and Cherniak, D. J. (2010) Diffusion in Minerals and Melts: Introduction. In *Diffusion in minerals and melts. Reviews in Mineralogy and Geochemistry*, **72**. Mineralogical Society of America, Washington, DC. pp. 1–4. https://doi.org/10.2138/rmg.2010.72.1

Zhang, Y. and Ni, H. (2010) Diffusion of H, C, and O Components in Silicate Melts. In *Diffusion in minerals and melts.* Reviews in Mineralogy and Geochemistry, **72**. Mineralogical Society of America, Washington, DC. pp. 171–225. https://doi.org/10.2138/rmg.2010.72.5

Zhang, Y. and Stolper, E. M. (1991) Water diffusion in a basaltic melt. *Nature* **351**, 306–309. https://doi.org/10.1038/351306a0

Zhang, Y., Ni, H. and Chen, Y. (2010) Diffusion Data in Silicate Melts. In *Diffusion in minerals and melts.* Reviews in Mineralogy and Geochemistry, **72**. Mineralogical Society of America, Washington, DC. pp. 311–408. https://doi.org/10.2138/rmg.2010.72.8

Zhang, L., Guo, X., Wang, Q., Ding, J. and Ni, H. (2017) Diffusion of hydrous species in model basaltic melt. *Geochim. Cosmochim. Acta* **215**, 377–386. https://doi.org/10.1016/j.gca.2017.07.019

Zoller, W. H., Parrington, J. and Phelan Kotra, J. (1983) Iridium enrichment in airborne particles from Kilauea volcano: January 1983. *Science* **222**, 4–7. https://doi.org/10.1126/science.222.4628.1118

Zreda-Gostynska, G., Kyle, P. R., Finnegan, D. L. and Prestbo, K. (1997) Volcanic gas emissions from Mount Erebus and their impact on the Antarctic environment. *J. Geophys. Res.* **102(B7)**, 15039–15055. https://doi.org/10.1029/97JB00155

Figure captions

Fig. 1. The effective (observed) partition coefficient *Kd** vs. the equilibrium partition coefficient *Kd* for elements distributing themselves between the surficial silicate melt and volcanic gas, depending on the ratios of the diffusion coefficient of an element X to the diffusion coefficient of water in the melt D_X/D_W. (a) Graph plotted taking into account the bubble expansion, Eqn. (7). (b), Graph for gas bubbles without taking into account the bubble expansion. The curve for the ratio of the diffusion rates $D_X/D_W = 0.01$ is relevant for a significant number of elements. The dashed curve shows the additional shift, taking into account a three-fold decrease in the water diffusion coefficient at a low water concentration in the melt. The graph in Fig. 1a demonstrates that the observed/equilibrium ratio Kd^*/Kd ~1 for most of the trace elements in volcanic gases, excepting the two most volatile elements Se and Te. The graphs are plotted for a water supersaturation ΔC_w of 0.2 wt. %.

Fig. 2. Ternary plot showing the molar abundances in coordinates 100HCl–H_2O–10S(tot) for volcanoes analyzed in this study. Gases from arc volcanoes are noticeably enriched in HCl and depleted in sulfur compared to rift/hotspot volcanoes. References for the data are the same as provided for Table 4.

Fig. 3. Total alkalis vs. silica (TAS) diagram for the volcanoes under the study.

Fig. 4. Spider diagram showing the elemental compositions separately for arc and rift/hotspot volcanoes under the study, which includes four arc volcanoes (Tolbachik, Masaya, Etna and Ambrym) and two rift/hotspot volcanoes (Erta-Ale and Kilauea) in descending order of the concentrations in Kilauea basalts. Data for REE normalized to chondrite C1 are shown as inset.

Fig. 5. Concentrations of the elements in volcanic gases vs. the corresponding concentrations in coexisting silicate melts. The aerosol fraction was excluded from the gas analyses. Elements with high and moderate volatility and high concentrations in the melt obey the partitioning law, at least partially: their concentrations in gas are roughly proportional to the concentrations in the coexisting melt. Different geochemical groups of elements are shown in different colors. The oncentrations of volatile elements (S, F, Cl, and Br) are taken from quenched basaltic glasses. The concentrations of B, Se, Cd, Re, and Bi in rocks are corrected for losses during degassing. For each of the elements, all points are combined into one field, regardless of the tectonic position of the volcano. The fields for antimony and nickel are shown with a dashed line, because the data for these elements are not reliable. Narrow vertical fields (Al, Fe, V, etc.) are due to the fact that these elements have approximately equal concentrations in the studied rocks.

Simultaneously, they demonstrate a large concentration range in the gas analyses, which are likely sampling and analytical artifacts.

Fig. 6. The concentrations of certain elements in gases can differ significantly depending on the tectonic position of the volcano, even if the concentrations of these elements are comparable or almost the same in the corresponding melts. Only elements with maximally different concentrations between arc and rift/hotspot settings are shown.

Fig. 7. Graphical representation of partition coefficients for the volcanic gas - silicate melt system in descending order, with uncertainties. Arc and rift/hotspot volcanoes are shown separately. (a) More reliable data (low uncertainties) and important elements with single analyses (Os, and Ir). (b) Elements with high uncertainties (1.5-3 orders of magnitude) and with single analysis.

Fig. 8. Partition coefficients *Kd* vs. enrichment factors *EF* on a log–log plot for the gas–melt system of the 2013 Tolbachik eruption. Ytterbium was used as a reference element, which provided $log\left(\frac{(C_{Yb})_{melt}}{(C_{Yb})_{gas}}\right)$ of 4.322. The logarithms of *Kd* and *EF* differ approximately by this value for most of the elements in the Tolbachik gases.

Fig. 9. Comparison of the partition coefficients *Kd* calculated for non-convective degassing (lava flows) and convective degassing (open–vent volcanoes). Only arc volcanoes (Tolbachik, Ambrym, Etna, Masaya) are used for comparison. Most symbols are located along the line corresponding to $Kd^{vent} / Kd^{flow} = 1$. The group of alkali metals and some chalcophile elements demonstrate slightly elevated ratios, being located close the line of $Kd^{vent} / Kd^{flow} = 3$. Elements with log (Kd) ≥ –3 and with low uncertainties in Kd (Table 5a) are included.

Partitioning of elements between high-temperature, low-density aqueous fluid and silicate melt as determined by volcanic gas geochemistry

Electronic Annex 1: Calculations and modeling

Part 1. Bubble growth at contrasting melt and fluid densities

Notation list

Symbol	Definition

A	distance from a flat surface boundary
Ar	Archimedes number $Ar = 8g\rho_m r_e^3/\eta$
C(r,t)	concentration of a component X in melt depending on radial coordinate and time
C_{fl}	concentration (wt. fraction) of a component X in fluid in the bubble
c_{fl}	concentration (wt. fraction) of a component X in the fluid incoming into the bubble
D_w	diffusion coefficient of water in melt
D_x	diffusion coefficient of a component X in melt
G	gravitational acceleration
Kd	equilibrium partition coefficient of a component X in the fluid/melt system
Kd*	apparent (measured) partition coefficient for a component X in the fluid/melt system
m_w	mass of water
m_x	mass of a component X
Pe	Peclet number; in the problem of the fast bubble expansion $Pe = r_b U_b/Dx$ for the component X and $Pe = r_b U_b/D_W$ for water
q_w	diffusion mass flux of water
q_x	diffusion mass flux of a component X
r	radial coordinate in the melt shell around the bubble
r_b	bubble radius
r_e	equivalent radius of a nonspherical bubble calculated from its volume
S	bubble surface
Sh	Sherwood number; equal to integrated diffusion flux on the boundary of the bubble moving in the melt, scaled on the $\Delta C D_X/2r_e$
t	time
U(r)	distribution of the radial melt flow rate at the bubble expansion
U_b	bubble growth rate
$\overline{D}_X$	relative diffusion coefficient of a component X (Dx/Dw)
ξ	nondimensional coordinate in the melt shell around the bubble
τ	time scaled on the diffusion time
ΔC_w	difference between far field and boundary concentrations of water
ΔC_x	difference between far field and boundary concentrations of a component X (C_0-C_b)
ρ_{fl}	density of fluid
ρ_m	density of melt

A. General considerations

Concentrations of elements measured in volcanic gases emitted during active eruptions can reflect equilibrium between low-density fluid and melt. They can also be constrained by determining the relative (against water) diffusion rate of components in the melt. Mass transfer of components from the melt into the bubble occurs via diffusion. The diffusive flux on the bubble (with radius growing with time $r_0(t)$) wall can be expressed through the concentration gradient as:

$$q_X = 4\pi r^2 \rho_m D_X \frac{\partial C_X(r,t)}{\partial r}\Big|_{r=r_0(t)} \qquad (1A).$$

The concentration gradient on the boundary is affected by bubble geometry and by the local melt flows. The flat boundary flux of a component X in the moment of time (t), can be easily expressed analytically by differentiation of the well-known solution via the following equation:

$C_{(z,t)} = C_0 + \Delta C_x erfc(\frac{z}{\sqrt{4tDx}})$, where *erfc* is the complementary error function that appears in many solutions of PDE: $erfc(x) = 1 - erf(x) = \frac{2}{\sqrt{x}} \int_x^\infty e^{-t^2} dt$

$$q_X = \frac{\Delta C_X \sqrt{D_X}}{\sqrt{\pi t}} \qquad (2A)$$

The ratio between the diffusive fluxes of water and component X (ratio of expressions (2A) for X and W(water)) is independent of time and can thus be calculated by:

$$q_X / q_W = \frac{\Delta C_X}{\Delta C_W} (D_X / D_W)^{1/2} \qquad (3A)$$

The spherical bubble vectors of the concentration gradient diverges (for plane they are parallel), and thus provides the existence of the stationary diffusive flux at the constant boundary and far-field concentrations $q_X = \Delta C_X D_X / r$ (where r is bubble radius). The value $q_0 = \Delta C_X D_X / 2r$ is used as a scale for fluxes of spherical bubbles in a flow field (as well as for non-spherical bubbles, when r is equivalent to the radius calculated from the bubble volume). Advective flow increases the concentration gradient by driving fresh melt to the bubble boundary, which accelerates the diffusion rate. Quasi-stationary diffusive transfer in the flow is described as the dependence of the Sherwood number $Sh = q_X / q_0 = f(Pe)$, where $Pe_X = r U_{flow} / D_X$. In this case, the fluxes ratio can be expressed with eqn. (4A) generalizing eqn. (3A)

$$q_X / q_W = \frac{\Delta C_X}{\Delta C_W} f(D_X / D_W), \qquad (4A)$$

where function f is expressed through the dependence of $Sh(Pe)$. In the present publication we consider the effect of the local flow caused by fast bubble growth (FBG) from the melt near the surface (approaching atmospheric pressures) of a lava flow. An extremely low fluid density results in high rates of bubble expansion, exceeding typical expansion rates for bubble growth at 10 – 100 MPa in a magma conduit (e.g., Proussevitch et al., 1993; Lyakhovsky et al., 1996), by several orders of magnitude. Independently of the nature of flow (e.g. flow around a rising bubble, shear flow near the dyke wall or advection flow around a growing bubble), general assumptions of the bubble composition can be made.

In general, the bulk concentration (C_{fl}) of a component X in the fluid (e.g. inside the bubble) changes in accordance with the following equation:

$$\frac{d(m_X/m_W)}{dt} = \frac{dm_X(t)}{dt}\frac{1}{m_W(t)} - \frac{m_X(t)}{m_W(t)^2}\frac{dm_W(t)}{dt} \text{ or } \frac{dC_{fl}}{dt} = \frac{(q_X - q_W C_{fl})}{m_W(t)} \qquad (5A);$$

with the assumption that $m_X << m_W$. When both fluxes are positive (diffusing into the bubble), their ratio q_X/q_W is equal to a current concentration of the component X in the incoming fluid c_{fl}. Therefore eqn. (5A) can be rewritten as:

$$\frac{dC_{fl}}{dt} = \frac{(c_{fl}(t) - C_{fl}(t))q_W}{m_W(t)} \qquad (6A).$$

This equation can then be solved for C_{fl}:

$$C_{fl} = \frac{\int_0^t q_W(\tau)c_{fl}(\tau)d\tau + C_0 m_0}{m_W(t)} \qquad (7A).$$

As such, the bulk fluid composition C_{fl} is averaged by the mass (m_W) of fluid instant concentration $c_{fl}(t)$. Here C_0 and m_0 are the composition and mass of the initial bubble (e.g. a bubble with the critical radius when capillary and viscous forces are essential).

Equation (6A) also has a stationary solution. Let us express the instant $c_{fl}(t)$ using Eqn. (5A) and setting the driving diffusion in the melt concentration increment as the difference between far-field and equilibrium boundary concentrations $\Delta C_X = (C_{0,X} - k_d \cdot C_{fl}(t))$. Here we assume local equilibrium between melt and fluid. The partition coefficient k_d (fluid-melt, small letters) is $1/Kd$, where Kd is a more convenient partition coefficient of melt-fluid. The stationary value of $C_{fl,ss}$ (stationary state is when incoming concentration is equal to the current bulk) can be solved by the linear equation:

$$c_{fl}(t) = q_X/q_W = \left(C_{0,X} - k_d \cdot C_{fl}(t)\right)/\Delta C_W f(D_X/D_W) = C_{fl} \text{ or}$$

$$C_{fl,SS} = C_{0,i}\frac{f(D_X/D_W)Kd}{f(D_X/D_W) + Kd \cdot \Delta C_w} \qquad (8A)$$

With time, fluid composition evolves to the stationary (indeed quasi-stationary) solution. This solution is stable in the sense that any deviation from it $\delta(t)$ is decaying. The solution for deviation $\delta(t)$ can be obtained by substituting the value $C_{fl,SS} + \delta(t)$ into equation (6A). It can be easily shown that:

$$\delta(t) = \delta_0\left(\frac{m_0}{m_w(t)}\right)^{\frac{f(Dx/Dw)}{Kd\Delta Cw}} \qquad (9A)$$

The ratio of the initial to the current moment t masses of water is <1, therefore the value of deviation from the stationary concentration reduces with time and proves the stability of the solution.

Obviously at the large relative diffusivity of the component X ($f(D_X/D_W) >> 1$), the apparent distribution coefficient $Kd^* = C_{fl}/C_{0,X} = Kd$, at a small diffusivity ratio is $f(D_X/D_W)/\Delta C_W$. Dependence of $f(D_X/D_W)$ is defined by the physical mechanism of mass transfer. It is easy to show this for slow bubble growth in a highly viscous melt (neglect flow) $f(D_X/D_W) = D_X/D_W$. For high Re flow (large bubbles with a

spherical cap shape in low viscosity melt) $J(D_X/D_W) = (D_X/D_W)^{1/2}$. Below we discuss the Fast Bubble Growth (FBG) model.

B. Fast bubble growth at near surface conditions

Bubble growth during degassing in near surface conditions proceeds in a specific dynamic regime, due to the extremely small density (0.0001 g/cm^3) of the water fluid at atmospheric pressure and high temperature. Owing to the low fluid density, the bubble growth rate is super-fast and thus melt flow around bubbles becomes essential for the diffusion mechanism. Below we briefly consider the effect of the melt advection on the fluid composition.

We start with analysis of the full equation for diffusive mass transfer around a bubble growing in an infinite melt volume. The growing bubble expands and causes radial melt flow, therefore the general mass balance equation can be written as:

$$\frac{\partial C(r,t)}{\partial t} = -U(r)\,\frac{\partial C(r,t)}{\partial r} + D\left(\frac{2\partial C/\partial r}{r} + \frac{\partial^2 C(r,t)}{\partial r^2}\right) \qquad (1B)$$

Or alternatively in coordinates relative to the rate U_b of the bubble boundary

$$\frac{\partial C(r,t)}{\partial t} - U_b\,\frac{\partial C(r,t)}{\partial r} = -U(r)\,\frac{\partial C(r,t)}{\partial r} + D\left(\frac{2\partial C/\partial r}{r} + \frac{\partial^2 C(r,t)}{\partial r^2}\right), \qquad (2B)$$

where D is the diffusion coefficient, and radial flow rate $U(r)$ is $U(r) = U_0 r_{02}(t)/r^2$, here $r_0(t)$ is radius of bubble. The growth rate of a bubble is controlled by the diffusive flux via the following equation:

$$\frac{\partial(4/3\pi r_0(t)^3 \rho_{fl})}{\partial t} = 4\pi r_0(t)^2 \rho_m D \frac{\partial C(r,t)}{\partial r}\Big|_{r=r_0(t)} \text{ or}$$
$$\frac{dr_0(t)}{dt} = \rho_m/\rho_{fl} D \frac{\partial C(r,t)}{\partial r}\Big|_{r=r_0(t)} \qquad (3B)$$

With scaling: time – $r_0(0)^2/D$, length $r_0(0)$ this equation can be expressed in moving with the bubble boundary coordinates ($\xi=(x-r_0(\tau))/r_0(0)$) as:

$$\frac{\partial C(\xi,\tau)}{\partial \tau} = Pe(\tau)\frac{\partial C(\xi,\tau)}{\partial \xi}\left(-\frac{r_0(\tau)^2}{(\xi+r_0(\tau))^2}+1\right) + \frac{\partial C(\xi,\tau)}{\partial \xi}\left(\frac{2}{\xi+r_0(\tau)}\right) + \frac{\partial^2 C(\xi,\tau)}{\partial \xi^2} \qquad (4B)$$

$$Pe(\tau) = \frac{dr_0(\tau)}{d\tau} = \rho_m/\rho_{fl}\left.\frac{\partial C(\xi,t)}{\partial \xi}\right|_{\xi=0} \qquad (5B)$$

where $0<\xi<\infty$. The effect of flow is defined by its relative intensity. It can be shown that at a moderate ratio of melt to fluid densities (pressures >100 MPa), the Peclet number is ≤0.1 and advection is no longer relevant. For small pressures and fluid densities, advection strongly affects the concentration field. The radial flow rate decreases as a $1/r^2$. Due to this effect, the distance between two arbitrary points reduces and therefore even a small concentration gradient sharpens with time. Diffusion dissipates the

concentration gradient and the integral effect depends on the *Pe* number that can be shown with quasi-stationary solution of eqn. (4B).

We set a linear scale to determine the bubble radius in the moment of time τ. $R_0=r_0(\tau)$ and we assume that concentration profile varies slowly: $\frac{\partial C(\xi,\tau)}{\partial \tau} \approx 0$. Then quasi-stationary solution (C(1+ζ)=C(r)) in the arbitrary moment of time τ as a function of *Pe* can be generally expressed as:

$$C(r) = c_1 + c_2 \int \exp\left(-\frac{Pe\ \xi^2 + 2\ln(\xi)\xi + Pe}{\xi}\right) d\xi \qquad (6B)$$

Quasi-stationary distribution of concentration near the bubble boundary, follows the increasing of the bubble radius preserving its shape as determined by equation (6B), with the linear scale depending on time. At *Pe*=0 equation (6B) transforms into the simple form widely used to derive the quasi-stationary concentration field around growing spherical crystals or bubbles:

$$C(r) = c_1 + \frac{c_2}{r} \qquad (7B)$$

By considering the difference between concentrations on the bubble wall and far field value, we set *C(1)=0, C(∞)=ΔC*, then c_1=0 and concentration can be expressed as:

$$C(r) = c_2 F(r) = c_2 \int_1^r \exp\left(-\frac{Pe\ \xi^2 + 2\ln(\xi)\xi + Pe}{\xi}\right) d\xi \qquad (8B)$$

The behavior of the profile near bubble wall can be studied with a series of decomposition functions in an exponent of eqn. (8B) near *r*=1. The series of decomposition function in integral eqn. (8B) around *Pe*=1 is:

$$f(r) = -((Pe-1)(r-1)^2 + 2(Pe+r) - 2) + 0(Pe-1)^3 \qquad (9B)$$

and *F(r)*:

$$F(r) = erf((rPe - Pe - r + 2)/\sqrt{Pe-1}) - erf(1/\sqrt{Pe-1}) \qquad (10B)$$

In eqn. 9B, "0" in the rightmost term shows an order of smallness, i.e. the ratio of expansion to the term $(Pe-1)^3$; $(Pe-1)^3 \rightarrow 0$ as $Pe \rightarrow 1$; expansion with accuracy up to quadratic terms.

The stationary profiles *C(r)* defined by the *F(r)* are depicted in Figure 1a.

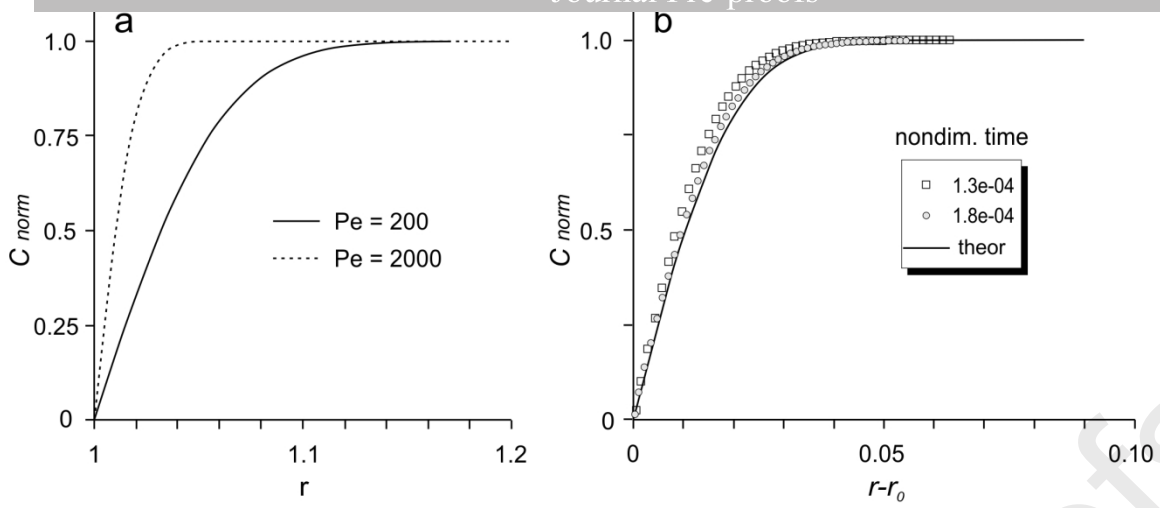

Fig. 1. Concentration profiles of $C(r)$. a) Stationary diffusion profile at different Pe; Pe=2000 corresponds to the density ratio as at the surface degassing. b) Full numerical (nondimensional time is labeled) and approximate analytical solutions at Pe=2000 (eqn. 8B).

Correctness of the numerical calculations and theoretical approximation (eqn. 8B) is confirmed (see Figure 1b).

By differentiation of eqn. (8B), the diffusion flux at r=1 is proportional to:

$$q \propto \exp(-1/(Pe-1))\sqrt{Pe-1} \qquad (11B)$$

The current radius is taken as a scale and it is assumed that it changes more slowly than the boundary layer is formed. Therefore, at the sufficiently large Peclet numbers (thin boundary layer), the diffusive flux is proportional to the square root of the diffusion coefficient D. Dependence of the stationary boundary layer thickness on Pe was evaluated from solutions of eqns. 8B-10B (Fig. 2).

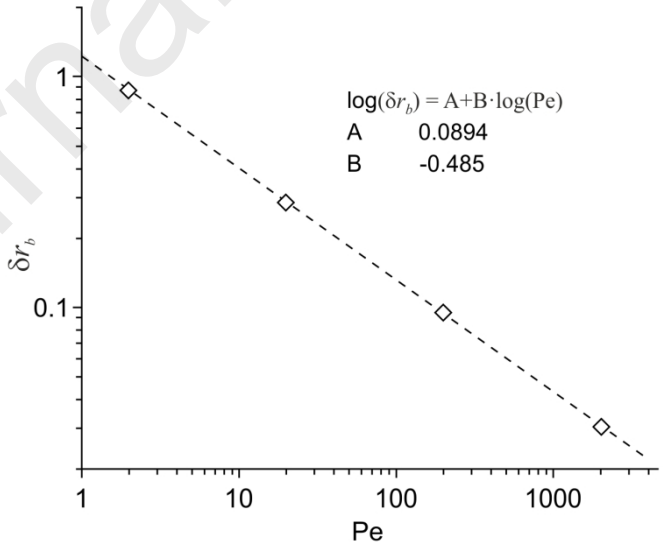

Fig. 2. Dependence of the boundary layer thickness on Peclet number, the stationary diffusion profile. The thickness of the boundary layer is defined as ($C(\delta r_b)$=0.95ΔC_0). The dependence is close to the square root.

Dependence of the relative bubble growth rate (*Pe*) on the modified density ratio $R_\rho = \Delta C \rho_{fl}/\rho_m$ is calculated and shown in Fig. 3.

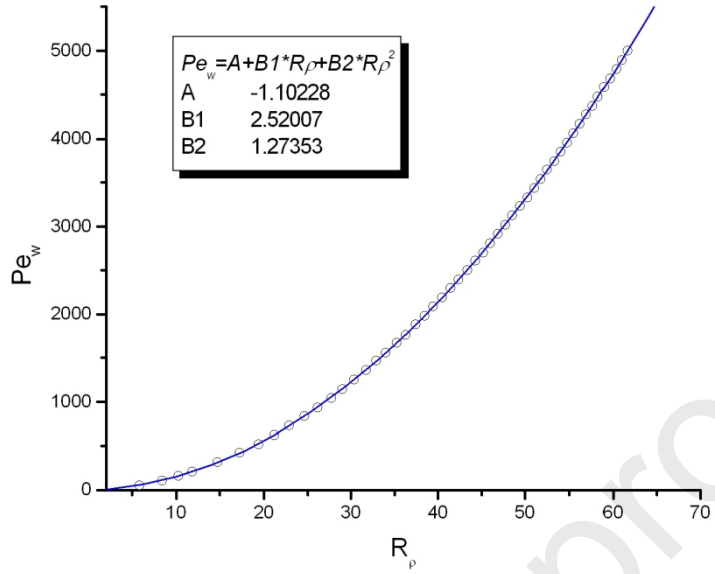

Fig. 3. Dependence of the normalized stationary bubble growth rate (*Pe*) from the modified density ratio $R_\rho = \Delta C_w \rho_{fl}/\rho_m$. Growth rate in the near surface magma flows is characterized by $R_\rho = 30–40$.

Thus, when bubble growth is in the regime of a fast boundary layer, the diffusion mass ratio of two components is proportional to the square root of their diffusivities. Whereas at slow growth rates ($Pe<<1$) it is proportional to the ratio of diffusivities.

Methods

Approximate analytical solution of the fast growing bubble problem was tested with numerical modeling results in the spherical shell geometry. A numerical solution was obtained by using the mesh-less inverse multi-quadric method (Cheng et al., 2003) on the Lagrange collocation points moving with the expanding shell. The Lagrange approach avoids problems with advection and is suitable for moving boundary problems such as bubble growth (e.g. Lyakhovsky, 1996). Mesh-less methods involve the approximation of the solution for the concentration with inverse multi-quadric global functions on the set of Lagrangian points. Approximated solution inserted in PDE of diffusion results in the linear problem relative coefficients of the probe functions with dense matrix.

Part 2. Transition from decompression to isobaric mode

Notation list

Symbol	Definition
α	Multiplier factor

A	Area
C	Concentration
C_S	Saturation concentration of
D	Diffusivity
h	Shell thickness
Kv	Volume partition coefficient
m	Mass
P	Density
R	Radius
T	Time
V	Volume
	Indices
B	Bubble
Fl	Fluid
I	Shell number
J	Time step j
melt	Melt
Sh	Shell
X	Component X

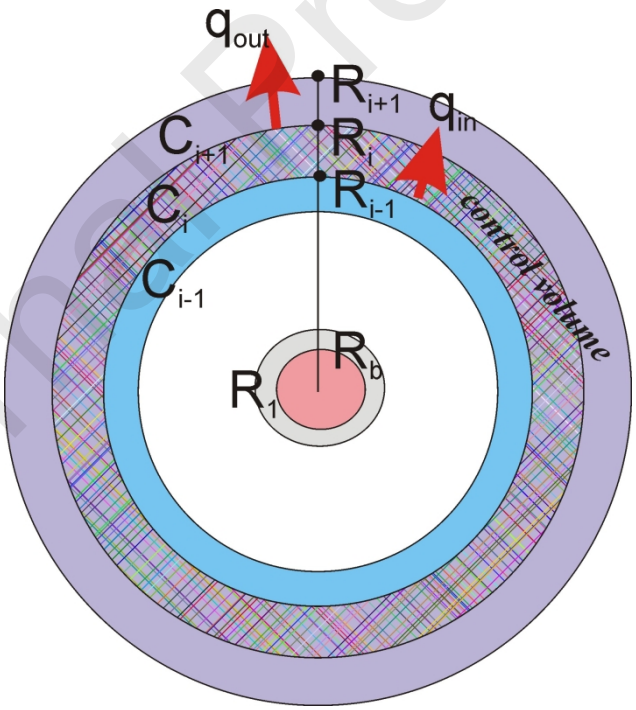

Fig. 4. Illustration for the control-volume method.

A numerical simulation following the control-volume method (Fig. 4), an alternative to a meshless one, was implemented to calculate the transitional time from the decompression degassing to the isobaric degassing with the steady state composition of the bubble in a wide range of diffusivities. In this method,

the diffusion equation is formulated as an integral mass balance for some domain from the set filling computation volume:

$$VdC_V / dt = \int_S (q \cdot n) ds\,, \qquad (1C)$$

Here the vector of the mass flux is multiplied by the vector of normal directed into the volume; the integral is calculated over the total surface. In our case of the spherical symmetry, the set of spherical shells is used (see Fig. 4) and this formula is reduced to the rather simple one:

$$V\Delta C_V / \Delta t = 4\pi(q_{in}R_{in}^{\ 2} - q_{out}R_{out}^{\ 2})\,, \quad C(t+\Delta t) = C(t) + 4\pi(q_{in}R_{in}^{\ 2} - q_{out}R_{out}^{\ 2})\Delta t / V \qquad (2C)$$

The diffusive flux is approximated with finite difference:

$$q_{in} = D(C_i - C_{i-1})/(r_i - r_{i-1}) \quad q_{out} = D(C_{i+1} - C_i)/(r_{i+1} - r_i) \qquad (3C)$$

Viscous flow is modeled in the Lagrange approach, i.e. control volumes (respective nodes) and expand in the radial flow with rate $U_m(r)$ satisfying the continuity equation as described in the text. The flow chart of the code follows that of Watson (2017). Initially uniform spacing of the CV (control volumes) grid was applied. During the bubble growth, inner nodes get closer. An explicit scheme was used, at the time step k+1:

1) Fluxes (in and out) of water and component X were calculated from the step k with eqn.(3B)

$q_{k+1} = Q(C_k, r_k)$

2) New concentrations are calculated in accordance with equation (2B)

3) At the bubble boundary, constant concentration of water is equal to its solubility. In the CV method this concentration is prescribed to the whole layer adjacent the fluid. To keep concentration constant $q_{out}=q_{in}$. Mass of water and the bubble radius is upgraded; the radius sets new position of the first node of the grid based on the constant volume condition:

$$m_{W,k+1} = m_{W,k+1} + D\frac{C_{1,k} - C_b}{r_{1,k} - r_b} A_{1,k}\Delta t \qquad (4C)$$

4) New positions of other nodes are calculated from the constant volume of the shells condition and calculations are returned to point 1.

Operations 1 – 4 are repeated for each time increment until the calculation is completed. During modeling, the calculations stopped when performing from 4000 to 20,000 time increments.

The described algorithm for the numerical calculation of a bubble growth under diffusion control is similar to the algorithm that was used to calculate diffusion fractionation by Watson (2017). The difference is that in our calculations, the growing bubble does not “consume” the melt as described by Watson (2017), but expands the melt instead. As a result, each of the spherical shells becomes thinner. The numerical calculation via repetitive operations 1-9 provides the same result as the numerical or

analytical solutions for the equation of diffusion into the growing bubble: $\frac{\partial C}{\partial t} + V_r \frac{\partial C}{\partial r} = \frac{1}{r^2}\frac{\partial}{\partial r}\left(Dr^2 \frac{\partial C}{\partial r} \right)$,

where V(r) is the radial rate of flow of the melt: $V = \frac{r_b^2}{r^2}\frac{dr_b}{dt}$; r changes from r_b to infinity (e.g., Proussevitch et al., 1993; Lyakhovsky et al., 1996).

The results of the simulation are summarized in Fig. 5. A bubble is instantly placed into initially homogeneous model melt. We simulated equilibration of a bubble with a 1 mm diameter and comprising concentrations of elements 10 times higher than the equilibrium concentrations. All equilibration curves have the same shape, but different time scales, the latter depending on the partition coefficient of the element in the "volcanic gas - silicate melt" system. Elements with low *Kd* (K, Pb) equilibrate within 10^{-6} – 10^{-3} s. Equilibration of elements with higher *Kd* (Br, Cd, Tl, Te) requires time from tenths of a second to several minutes. It is also clearly seen on a logarithmic scale that the equilibration process is initially fast, and then gradually slows down.

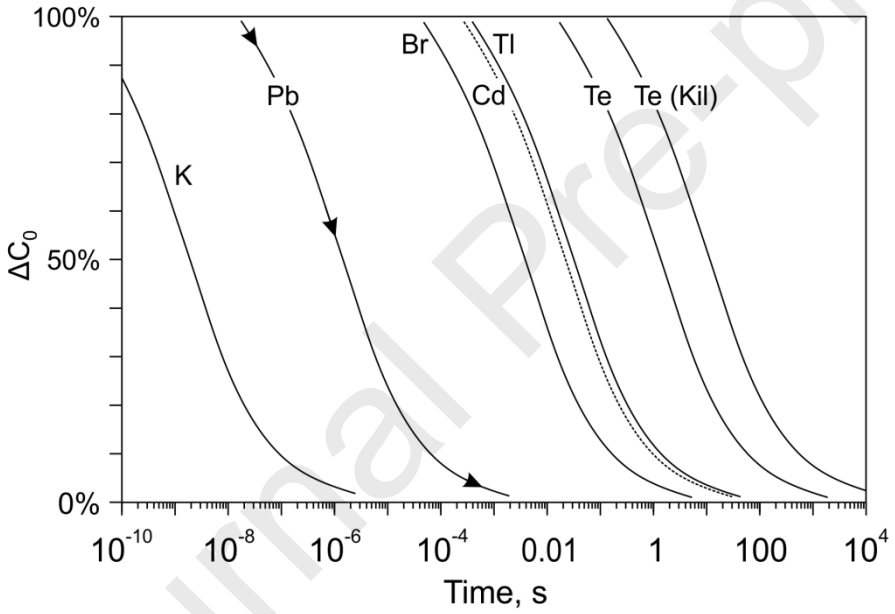

Fig. 5. A plot showing evolution of concentrations vs. time during equilibration of a model bubble 1 mm in diameter with arbitrary initial concentrations of elements. A similar process takes place after transition of the bubble growth mode from decompression to isobaric (from vertical magma ascent to horizontal lava flow). The vertical axis of the plot (ΔC_0) expresses the difference between the initial concentration and the equilibrium concentration of an element.

The diffusive degassing from the free melt surface was modelled as non-stationary diffusion in a semi-infinite medium. The simulation algorithm was similar to the simulation of diffusion into a bubble, but flat layers of constant thickness were used for the calculation instead of spherical geometry. The concentration of a component X in the gas phase adjacent to the melt surface was maintained at equal to

zero, since the limiting case, in which the external diffusion boundary layer is absent, was adopted for the model.

References

Cheng, A. H.-D., Golberg, M. A., Kansa, E. J., Zammito, G. (2003) Exponential convergence and H-c multiquadric collocation method for partial differential equations. Numerical Methods in Partial Differential Equations 19, 571-594. https://doi.org/10.1002/num.10062

Lyakhovsky, V., Hurwitz, S., & Navon, O. (1996). Bubble growth in rhyolitic melts: Experimental and numerical investigation. Bull. Volcanol. 58, 19–32. https://doi.org/10.1007/s004450050122

Proussevitch, A. A., Sahagian, D. L., & Anderson, a. T. (1993). Dynamics of diffusive bubble growth in magmas: Isothermal case. Journal of Geophysical Research, 98(B12), 22283. https://doi.org/10.1029/93JB02027

Watson, E. B. (2017) Diffusive fractionation of volatiles and their isotopes during bubble growth in magmas. Contrib. Mineral. Petrol. 172, 1–21. https://doi.org/10.1007/s00410-017-1384-7

Partitioning of elements between high-temperature, low-density aqueous fluid and silicate melt as determined by volcanic gas geochemistry

Electronic Annex 2: Volcanic rock and gas composition data

Volcanic rock composition data

Rock analysis is a well-established procedure, with thousands of laboratories processing millions of samples annually. The data quality can be verified on standard samples, which are repeatedly analyzed in different laboratories and as a result, the compositions of the standards are carefully determined. Nevertheless our experience has shown that published analyses need to be thoroughly inspected prior to use for the calculation of partition coefficients. This is especially true for elements with low concentrations, which are rarely determined in common rock analyses (Se, Te, Ag, Cd, In, Au, platinum group elements).

A maximum of 60–62 elements can be determined simultaneously in a single series of decomposition and analysis procedures by the ICP-MS method. The completeness of the transfer of elements from the rock to the solution depends on the decomposition scheme used. The modern decomposition methods with 4 acids (e.g., Karandashev et al., 2008) make it possible to transfer into solution almost all elements even from low soluble minerals such as chromite. However, elements with low concentrations (e.g. Ag, Cd, Bi, Ge) often fall below the detection limit, and additional analyzes may be required to identify them. Indium is often used as an internal standard and is not shown in the analysis. As a rule, additional independent measurements are required to determine: (1) mercury; (2) bromine and iodine; (3) selenium and tellurium; (4) precious metals - Au, Ru, Rh, Pd, Ir, Pt; (5) Os and Re. Thus, in order to determine 70–74 metallic and non-metallic elements in a rock, it is necessary to perform not one, but rather 6–8 different analyzes. Only a few rocks on Earth are characterized by a complete set of elements analyzed. These include rocks used as reference materials, for example, BHVO-1.

Misprints and outliers may also occur in published data. The only way to detect anomalous analyzes is to compare them with the concentrations in similar rocks (e.g. arc basalts) from different volcanoes. For comparison, we selected (possibly somewhat arbitrarily) the following criteria. If the concentration of the element of interest is approximately equal in similar volcanic rocks from comparable geodynamic settings, it is likely that the element is determined accurately. If the concentration of element of interest differs by more than 3 times (± 0.5 orders of magnitude), it is likely that the element was not accurately measured. In the latter case, we replaced the anomalous analyses with the known concentration of this element in rocks of similar composition from volcanoes of the same tectonic setting.

Concentrations of F, S and Cl for the present paper were measured directly in quenched basaltic glasses (fine ash from Tolbachik, Pele's tears from Erta-Ale and Masaya; de Moor et al., 2013; Zelenski et al., 2014; Plechov et al., 2015). Data on sulfur content in basaltic spatter and Pele's hair from Kilauea can be found in Katsura and Nagashima (1974), who studied the solubility of sulfur in mafic magmas at 1 bar. They found an average S content of 180 ppm for most samples, which as a first approximation, reflect sulfur content in surficial silicate melts and is almost twice as high as S content in the BHVO-1 standard. Reliable data for Etna basaltic scoria for S and Cl content were taken from Metrich and Clocchiatti (1989).

Not only F, S and Cl escape melt during degassing, concentrations of some metallic and non-metallic trace elements such as B, Se, Cd, Re and Bi may also significantly decrease during this process. In order to avoid the impact of this effect, rock analyses were corrected for losses during degassing. This was done according to emanation coefficients (Lambert et al., 1985). This coefficient stands for the fraction of an element to be expelled from the melt during degassing. Emanation coefficients for B, Se and Cd were taken from Rubin (1997) and for Re and Bi from Norman et al. (2004). Correction for losses for elements having emanation coefficient < 10% such as Te and Tl is negligible due its small influence on the calculated *Kd*. According to Rubin (1997), these elements have emanation coefficients << 1%, although data from Edmonds et al (2018) suggest they may be highly volatile in volcanic conditions.

The corrected concentrations of elements in volcanic rocks of the six volcanoes studied expressed in ppm, are given in Supplementary Table S1. References to the data sources are given in the footnotes of the tables. Additional data for possible corrections were taken for each of the volcanoes directly from the GEOROC database.

Some data on the concentration of metals in rocks were obtained in the course of the present study. This includes data on osmium, iridium and gold for basalt from Erta Ale volcano and data on gold for Tolbachik volcano. Iridium and gold were analyzed in the commercial laboratory Geolabs in Sudbury, Canada with a pre-concentration Fire Assay method with NiS, followed by conventional ICP-MS. Osmium was analyzed using an isotope dilution method in Novosibirsk, Russia, Institute of Geology and Mineralogy.

Volcanic gas composition data

The compositions of volcanic gases in terms of major gas species are well studied to date (e.g., reviews by Symonds et al., 1994; Fischer and Chiodini, 2015). Main components of high-temperature volcanic gas (which are separated directly from magma) are water vapor (H_2O) followed by CO_2 or SO_2. Such compounds as H_2S, HCl and HF rarely exceed 1-3 mol. %. The ratios between H_2O, S, and HCl depend on the tectonic position of the volcano. Arc gases are relatively enriched in HCl with S/Cl molar ratio < 10, whereas gases from intraplate and rift volcanoes contain much more SO_2, where it can reach 40 mol. % (Fig. 4).

Abundances and speciation of trace elements in volcanic gases are by far less studied than major gas species. Basic knowledge about the trace elements in volcanic emissions was obtained using either filter

pack sampling or direct collection of the gas condensate. The number of such analyses worldwide does not exceed a few dozen per year, and the procedure of trace elements measurements in such samples is not well elaborated.

Large dispersion of trace element data in volcanic gases is a much more significant problem for calculating partition coefficients than data inaccuracy for rocks. Unfortunately, a significant amount of data on the composition of volcanic gases is not very accurate. There are no special studies on this topic. Also, there are no standards by which it would be possible to check and calibrate the collected volcanic gas samples. Low metal concentrations and technical difficulties in sampling and analysis may cause analytical biases, typically toward the overestimation of element concentrations. Concentrations of the same element measured in the gas, in samples taken at the same volcano under approximately the same conditions, can be in the range reaching 4 orders of magnitude (e.g. Kilauea volcano). Similarly, the compositions of the melts, judging by the analyses of lavas, are approximately the same, as well as the compositions of gases in terms of the major gas species, which can be measured with acceptable accuracy. This topic is huge, almost inexhaustible and very complex. It is almost impossible to cover it in this article. All we could do was to select six works in which gas-melt pairs are more or less consistent with each other. Comparison of element concentrations from these selected works enabled us to calculate the partition coefficients with accuracy within half an order of magnitude at best, and considering difficulties with the trace element analysis in volcanic gas, we think that this is a good accuracy.

The main uncertainties for trace element composition measurements in volcanic gas arise for the following reasons:

(1) The presence of aerosol, which may have the same composition or be different from that of the silicate melt. The widely used approaches of "Enrichment Factor" (EF; Lepel et al., 1978; Zoller et al., 1983) or "Weight Ash Fraction" (WAF = 1/EF, Aiuppa et al., 2003) satisfactorily determine the amount of aerosol fraction only if the aerosol has exactly the same composition as the parent melt.

(2) Fractionation of elements before gas escapes to the atmosphere (partial deposition in fumarole channel) or during sampling (condensation inside a sampling line).

(3) Fractionation of elements after sampling due to sedimentation of colloidal sulfur in the gas condensate and adsorption of elements on sulfur particles or walls of a vial (Fischer et al., 1998).

(4) A large concentration range of simultaneously analyzed elements, sometimes exceeding 8 orders of magnitude, causes a matrix effect when the elements in high concentration (sulfur, chlorine) require dilution of the sample, thus reducing the sensitivity of the method to the most rare elements (Fischer et al., 1998, Karandashev et al., 2008).

(5) High laboratory blanks is a problem for analyzing of aerosol on filters due to low concentrations of metals in such aerosols.

(6) Dissolution of glassware of a sampling line during direct gas sampling and laboratory glassware when analyses are being undertaken. Acid gas condensate contains hydrofluoric acid (HF), which easily dissolved borosilicate glass so adding uncontrolled amounts of boron, silicon and some other elements to the analyzed condensate. In addition to sampling and analytical glassware components, there are still many sources of boron contamination. For example, purified acids used for ICP-MS works are contained in borosilicate glass bottles.

(7) Contamination from metallic instruments or plastic labware. Tweezers made of titanium or stainless steel may contaminate filter samples with Ti, Cr and Ni. Polypropylene (PP) vials or polyethylene terephthalate (PET) bottles that are commonly used for keeping gas condensate and other liquids during gas sampling and analysis commonly contain traces of catalyst used in polymerization. For

example, a Ziegler-Natta catalyst widely used for PP production may contain Ti, Zr and Hf, whereas PET bottles contain notable amount of leachable Sb (e.g., Keresztes et al., 2009). Contamination from instruments or plastic labware is more probable when working with filters due to low concentrations of elements on the latter.

(8) Memory effect of ICP-MS devices and polyatomic interferences (e.g., Karandashev et al., 2008, and references therein).

(9) Many of the previous analyses of aerosol filters performed by the INAA method may be overestimated by many times. For example, the X/SO_2 ratios for chalcophile elements in the plume of the Kilauea volcano, measured by INAA in aerosol samples collected from 1984 to 1996 (Hinkley at al., 1999), are 2-15 times greater than the similar ratios in aerosol of the 2008 eruption measured by ICP-MS (Mather et al., 2012). For thallium and bismuth the difference in the cited works reaches 65 and 437 times, respectively. Although such fluctuations of the elements are possible in principle, it is much more likely that the recent analyzes performed by the modern methods are just more accurate.

Problems (5) - (8) may be partially solved by blank analyzes. Problems (2), (3) and (4) are relevant only for condensates. The matrix effect (problem 4) occurring due to large range of concentrations can be eliminated by repetitive analyses of the same sample taken with different dilution factors. Finally, serial sampling makes it possible to identify those elements that are present in the gas or aerosol plume in the form of a non-silicate aerosol (solution to problem 1). As far as the mentioned problems can be solved only partially, the analyzed trace element concentrations and X/SO_2 ratios in volcanic gas samples vary within several orders of magnitude, even if done for the same volcano at the same conditions (e.g., compare data from Hinkley at al., 1999 and Mather et al., 2012; Kilauea volcano).

An important issue is the quality of analytical data, the dispersion of which for volcanic gas analyses is significant (Zelenski et al., 2013). Considering the absence of experimental data and standards, the only reliable way to evaluate quality of published data on the trace element in volcanic gases is to compare them with other analyses from the same or from other similar volcanoes. At least it is true for volcanoes located within the same tectonic position, which rocks and major gas species are similar.

After representative analyzes of rocks and volcanic gases were selected, we subtracted the aerosol fraction ("weight ash fraction as was suggested by Aiuppa et al., 2003) from the gas analyses using the formula WAF = $\frac{(C_X/C_R)_{rock}}{(C_X/C_R)_{gas}}$, where *X* stands for the element of interest and *R* and is the reference element. The fraction of an element initially emitted as gaseous species can be written as "1-WAF". The corrected concentrations of elements in volcanic gases of the six volcanoes under the study expressed in ppm are given in Supplementary Table S2.

Supplementary Table S1. Corrected concentrations of elements in rock analyses, ppm.

Element	Ambrym[1]	Erta-Ale[2]	Etna[3]	Kilauea[4]	Masaya[5]	Tolbachik[6]
Li		4.3	15.8	4.6	10.4	15.7
Be		0.93	1.30	1.04	0.80	1.72
B		4.6	12.2	3.8	33.7	91
F		678	650	474	367	605
Na	20475	20200	27100	16766	20600	27721
Mg	24612	39900	30700	43613	27421	24169
Al	88010	90400	96000	73033	80781	86370

Si	239400	228000	228667	232502	239060	243725
P	1572	1250	2539	1192	1180	3275
S		113	123	180	31.5	64
Cl		302	1575	132	557	595
K	16188	4450	15400	4317	10204	20643
Ca	63679	86900	74200	81475	68579	51722
Sc		36.9	20.0	31.8	38.1	21.7
Ti	5935	12100	6300	16246	6973	11487
V	301	304	305	317	384	318
Cr	20	95.7	32	291	40.6	34
Mn	1471	1330	1000	1317	1735	1404
Fe	90713	69400	77200	85546	91342	80557
Co	29.0	38.5	29.5	45.0	34.8	30.1
Ni	24	64.5	54	120	22	39
Cu	163	126	124	136	263	366
Zn	83	80.4	110	105	118	118
Ga	17.3	19.3	16	21	19.5	20.5
Ge	1.4	1.4	1.6	1.6		0.51
As	5.9	1.8	7.5	0.52	1.7	9.3
Se		0.11	0.033	0.11		0.033
Br		2.34	9	1.42		4.6
Rb	33	10.8	40.3	11	24	69.4
Sr	582	261	1130	403	436	324
Y	15.2	24.8	27.6	28	26.4	39.7
Zr	63	170	210	179	107	275
Nb	1.92	36.2	40.7	19	3.5	8.8
Mo	1.29	1.2	3.7	1.03	1.1	6.4
Ru		0.00017		0.00022		0.00011
Rh		0.00022		0.00011		0.00005
Pd		0.0059		0.0031		0.0058
Ag		0.06	0.045	0.054		0.183
Cd		0.20	0.20	0.13	0.15	0.12
In		0.07	0.08	0.088		0.069
Sn	1	1.33	1.5	1.93	1	1.76
Sb		0.1	0.12	0.16	0.29	0.47
Te	0.0071	0.0055	0.0018	0.0057	0.011	0.004
Cs	1.5	0.14	0.8	0.10	0.91	2.14
Ba	343	118	680	139	868	582
La	9	20	54	16	9.3	19.3
Ce	20.3	43.8	106	39	25.0	46.7
Pr	2.7	5.37	11.9	5.4	3.8	6.9
Nd	12.6	22.8	46.8	25	17.5	31.6
Sm	3.2	5	8.5	6.2	4.2	7.6
Eu	1.03	1.55	2.65	2.1	1.3	2.0
Gd	3	5.2	7.41	6.4	4.5	7.5
Tb	0.46	0.77	0.99	0.96	0.69	1.1
Dy	2.7	4.69	5.5	5.20	4.35	7.0
Ho	0.55	0.94	0.98	0.99	0.88	1.38
Er	1.54	2.59	2.49	2.4	2.52	4.0
Tm	0.23	0.35	0.33	0.33	0.38	0.58
Yb	1.5	2.29	2.04	2.0	2.37	3.79
Lu	0.24	0.33	0.32	0.29	0.36	0.56
Hf	1.83	3.93	4.55	4.4	2.59	6.43
Ta	0.16	1.75	2.58	1.2	0.18	0.47
W		1.02	1.9	0.27	0.31	0.91
Re		0.0016	0.0011	0.00093		0.0013
Os		0.00005		0.000084		

Ir		0.00017		0.000085		0.00006
Pt		0.0044	0.004	0.0031		0.0031
Au		0.0015	0.003	0.0017		0.0039
Hg		0.020	0.04	0.0048		0.37
Tl		0.035	0.09	0.043	0.092	0.12
Pb	6.3	1.55	8	2.6	3.7	7.5
Bi		0.029	0.065	0.022	0.033	0.052
Th	1.3	2.32	8.6	1.1	1.73	2.63
U	0.46	0.63	2.5	0.417	1.41	1.65

References: 1 – Allard et al., 2016; 2 – Zelenski et al., 2013, de Moor et al., 2013, data on osmium and iridium – this work; 3 – Aiuppa et al., 2003; 4 – Gladney and Roelandts, 1988; Lassiter, 2003; Verma et al., 2017; 5 – Martin et al., 2012; 6 – Zelenski et al., 2014; Plechov et al., 2015; data on gold – this work.

Supplementary Table S2. Corrected concentrations of elements in gas analyses, ppm.

Element	Ambrym[7]	Erta-Ale[8]	Etna[9]	Kilauea[10]	Masaya[11]	Tolbachik[12]
Number of data points for the each average value	5	8	9	3	29	11
Li		0.016		0.16	0.17	0.13
Be		0.00032		0.028	0.033	0.00047
B		0.27		33.7		1.90
F	1127	3389	5996	1541	1591	4898
Na		132	346	33.5		223
Mg						
Al	1756		4445	44.1	43.7	3.8
Si		99				62
P		0.23		1.50		0.074
S	24841	131901	40468	187993	29051	35940
Cl	4676	4474	48458	3075	14514	24741
K		70	779	32		249
Ca				30.2	114	2.3
Sc						0.0056
Ti						
V	0.384	0.032		0.016	0.074	0.029
Cr	16.0	0.0024		5.3		0.012
Mn		0.14	10.9	0.16	0.87	0.25
Fe	56.3	26.1		4.9	72.5	8.6
Co	0.067	0.011	3.0	0.056	0.016	0.0085
Ni		0.028		17.2		0.0071
Cu	6.6	4.6	52.7	1.9	26.4	21.0
Zn	2.3	4.3	9.8	20	8.5	4.7
Ga		0.023	0.6	0.023	0.012	0.00007
Ge		0.062		0.27		0.010
As	1.9	2.7	3.4	0.5	7.9	7.6
Se	2.3	5.4	5.14	34.8	0.13	1.6
Br	17.9	26	61.3	11.9		48
Rb	0.58	0.35	4.70	0.050	1.15	1.0
Sr				0.041	0.74	0.018
Y				0.0069	0.0072	
Zr				0.12		0.0079

Nb					0.0026		0.014
Mo			0.091	0.26	0.088	0.042	0.16
Ru							
Rh							
Pd							
Ag		0.15	0.022	0.06			0.011
Cd		0.28	6.8	1.4	2.0	1.0	0.66
In			0.15	0.22	0.04		0.075
Sn		7.65	0.40		2.0		0.094
Sb			0.009	30.6	0.046	0.050	0.009
Te			4.0	0.14	2.4	0.81	0.33
Cs		0.08	0.0095	0.27	0.0036	0.11	0.102
Ba		2.18	0.013		0.19	1.1	0.182
La		0.09			0.0080	0.022	0.0020
Ce					0.0018	0.024	0.0034
Pr						0.0033	0.000051
Nd						0.0096	
Sm						0.0018	
Eu			0.00012			0.00031	
Gd						0.00095	
Tb						0.00007	
Dy						0.00063	
Ho						0.00011	
Er						0.00019	
Tm						0.000013	
Yb							
Lu					1.6E-05		
Hf			0.00011		0.0017		0.0006
Ta			0.00024		0.0031		0.0066
W			0.0023		0.0064		0.0067
Re			0.061	0.027	0.050		0.024
Os			0.00061				
Ir			2.2E-05				
Pt			0.00075	0.0011			0.0004
Au		0.029	0.0023	0.012			0.0049
Hg		0.53	6.9E-05	0.11			
Tl		1.10	0.27	4.9	0.073	1.4	1.70
Pb		0.55	1.1	6.6	1.4	1.2	0.74
Bi		0.22	0.43	0.80	0.11	0.50	0.53
Th			5.0E-05		0.00083	0.0053	0.0018
U		0.057		0.022	0.00099	0.035	

References: 7 – Allard et al., 2016; 8 – Zelenski et al., 2013; 9 – Aiuppa et al., 2003; 10 – Mather et al., 2012; 11 – Martin et al., 2012; 12 – Zelenski et al., 2014.

Supplementary Table S3. Logarithms of calculated partition coefficients, log *Kd**.

Element	Ambrym	Erta-Ale	Etna	Kilauea	Masaya	Tolbachik
Li		-2.42		-1.47	-1.79	-2.08
Be		-3.47		-1.56	-1.38	-3.56
B		-1.24		0.94		-1.68
F		0.70	0.96	0.51	0.64	0.91
Na		-2.19	-1.89	-2.70		-2.10
Mg						
Al	-1.70		-1.33	-3.22	-3.27	-4.36
Si		-3.36				-3.60

P		-3.73		-2.90		-4.64
S		3.07	2.52	3.02	2.96	2.75
Cl		1.17	1.49	1.37	1.42	1.62
K		-1.80	-1.30	-2.13		-1.92
Ca				-3.43	-2.78	-4.36
Sc						-3.59
Ti						
V	-2.89	-3.98		-4.29	-3.71	-4.04
Cr	-0.10	-4.60		-1.74		-3.44
Mn		-3.96	-1.96	-3.92	-3.30	-3.74
Fe	-3.21	-3.42		-4.24	-3.10	-3.97
Co	-2.63	-3.54	-1.00	-2.91	-3.33	-3.55
Ni		-3.36		-0.84		-3.74
Cu	0.04	0.04	0.42	0.01	0.10	0.06
Zn	-1.56	-1.27	-1.05	-0.72	-1.14	-1.40
Ga		-2.92	-1.46	-2.96	-3.21	-5.49
Ge		-1.36		-0.77		-1.72
As	-0.50	0.17	-0.34	-0.05	0.67	-0.09
Se		1.70	2.19	2.52		1.70
Br		1.04	0.83	0.92		1.02
Rb	-1.75	-1.49	-0.93	-2.34	-1.32	-1.84
Sr				-3.99	-2.77	-4.26
Y				-3.61	-3.56	
Zr				-3.17		-4.54
Nb				-3.87		-2.81
Mo		-1.12	-1.15	-1.07	-1.42	-1.60
Ru						
Rh						
Pd						
Ag		-0.43	0.15			-1.22
Cd		1.53	0.85	1.18	0.83	0.74
In		0.33	0.44	-0.36		0.04
Sn	0.88	-0.52		0.02		-1.27
Sb		-1.04	2.41	-0.54	-0.76	-1.74
Te		2.86	1.89	2.63	1.85	1.91
Cs	-1.25	-1.17	-0.47	-1.46	-0.91	-1.32
Ba	-2.20	-3.95		-2.87	-2.89	-3.50
La	-1.99			-3.30	-2.62	-3.99
Ce				-4.33	-3.02	-4.14
Pr					-3.06	-5.13
Nd					-3.26	
Sm					-3.36	
Eu		-4.12			-3.64	
Gd					-3.67	
Tb					-3.99	
Dy					-3.84	
Ho					-3.91	
Er					-4.13	
Tm					-4.46	
Yb						
Lu				-4.26		
Hf		-4.57		-3.42		-4.06
Ta		-3.86		-2.58		-1.85
W		-2.64		-1.62		-2.14
Re		1.59	1.40	1.72		1.28
Os		1.09				
Ir		-0.88				

Pt		-0.76	-0.57			-0.83
Au		0.19	0.59			0.10
Hg		-2.46	0.45			
Tl		0.88	1.74	0.23	1.18	1.14
Pb	-1.06	-0.14	-0.08	-0.26	-0.50	-1.01
Bi		1.18	1.09	0.72	1.18	1.01
Th		-4.66		-3.12	-2.52	-3.16
U	-0.91		-2.05	0.00	-1.60	

References

Aiuppa, A., Dongarra, G., Valenza, M., Federico, C. and Pecoraino, G. (2003). Degassing of trace volatile metals during the 2001 eruption of Etna. Geophysical Monograph 139, 41–54. https://doi.org/10.1029/139GM03

Allard, P., Burton, M., Sawyer, G. and Bani, P. (2016). Degassing dynamics of basaltic lava lake at a top-ranking volatile emitter: Ambrym volcano, Vanuatu arc. Earth Planet. Sci. Lett. 448, 69–80. https://doi.org/10.1016/j.epsl.2016.05.014

de Moor, J. M., Fischer, T. P., Sharp, Z. D., King, P. L., Wilke, M., Botcharnikov, R. E., Cottrell, E., Zelenski, M., Marty, B., Klimm, K., Rivard, C., Ayalew, D., Ramirez, C. and Kelley, K. A. (2013). Sulfur degassing at Erta Ale (Ethiopia) and Masaya (Nicaragua) volcanoes: Implications for degassing processes and oxygen fugacities of basaltic systems. Earth Planet. Sci. Lett. 14, 4076–4108. https://doi.org/10.1002/ggge.20255

Edmonds, M., Mather, T. A. and Liu, E. J. (2018). A distinct metal fingerprint in arc volcanic emissions. Nat. Geosci. 11, 790-794. https://doi.org/10.1038/s41561-018-0214-5

Fischer, T. P. and Chiodini, G. (2015). Volcanic, Magmatic and Hydrothermal Gases. The Encyclopedia of Volcanoes (Second Edi). Elsevier Inc. https://doi.org/10.1016/b978-0-12-385938-9.00045-6

Fischer, T. P., Shuttleworth, S. and O'Day, P. A. (1998). Determination of trace and platinum-group elements in high ionic-strength volcanic fluids by sector-field inductively coupled plasma mass spectrometry (ICP-MS). Fresenius J. Anal. Chem. 362, 457–464. https://doi.org/10.1007/s002160051106

Gladney, E. S. and Roelandts, I. (1988) 1987 compilation of elemental concentration data for USGS BHVO-1, MAG-1, QLO-1, RGM-1, SCo-1, SDC-1, SGR-1, and STM-1. Geostand. Geoanal. Res. 12, 253–362. https://doi.org/10.1111/j.1751-908X.1988.tb00053.x

Hinkley, T. K., Lamothe, P. J., Wilson, S. A., Finnegan, D. L. and Gerlach, T. M. (1999). Metal emissions from Kilauea, and a suggested revision of the estimated worldwide metal output by quiescent degassing of volcanoes. Earth Planet. Sci. Lett. 170, 315–325. https://doi.org/10.1016/S0012-821X(99)00103-X

Karandashev, V. K., Turanov, A. N., Orlova, T. A., Lezhnev, A. E., Nosenko, S. V., Zolotareva, N. I. and Moskvitina, I. R. (2008). Use of the Inductively Coupled Plasma Mass Spectrometry. Inorg. Mater. 44(14), 1491–1500. https://doi.org/10.1134/S0020168508140045

Katsura, T. and Nagashima, S. (1974). Solubility of sulfur in some magmas at 1 atmosphere. Geochim. Cosmochim. Acta 38(4), 517–531. https://doi.org/10.1016/0016-7037(74)90038-6

Keresztes, S., Mihucz, V. G., Virág, I., Majdik, C. and Záray, G. (2009). Science of the Total Environment Leaching of antimony from polyethylene terephthalate (PET) bottles into mineral water. Sci. Total Environ. 407, 4731–4735. https://doi.org/10.1016/j.scitotenv.2009.04.025

Lambert, G., Le Cloarec, M. F., Ardouin, B. and Le Roulley, J. C. (1985). Volcanic emission of radionuclides and magma dynamics. Earth Planet. Sci. Lett. 76, 185–192. https://doi.org/10.1016/0012-821X(85)90158-X

Lassiter, J. C. (2003). Rhenium volatility in subaerial lavas: constraints from subaerial and submarine portions of the HSDP-2 Mauna Kea drillcore. Earth Planet. Sci. Lett. 214, 311-325. https://doi.org/10.1016/S0012-821X(03)00385-6

Lepel, E. A., Stefansson, K. M. and Zoller, W. H. (1978). The enrichment of volatile elements in the atmosphere by volcanic activity: Augustine Volcano 1976. J. Geophys. Res. 83, 6213–6220. https://doi.org/10.1029/JC083iC12p06213

Martin, R. S., Sawyer, G. M., Day, J. A., LeBlond, J. S., Ilyinskaya, E. and Oppenheimer, C. (2012). High-resolution size distributions and emission fluxes of trace elements from Masaya volcano, Nicaragua. J. Geophys. Res. 117(B8), 1–12. https://doi.org/10.1029/2012JB009487

Mather, T. A., Witt, M. L. I., Pyle, D. M., Quayle, B. M., Aiuppa, A., Bagnato, E., Martin, R.S., Sims, K. W. W., Edmonds, M., Sutton A. J. and Ilyinskaya, E. (2012). Halogens and trace metal emissions from the ongoing 2008 summit eruption of Kīlauea volcano, Hawai`i. Geochim. Cosmochim. Acta 83, 292–323. https://doi.org/10.1016/j.gca.2011.11.029

Metrich, N. and Clocchiatti, R. (1989). Melt inclusion investigation of the volatile behaviour in historic alkali basaltic magmas of Etna. Bull. Volcanol. 51, 185–198. https://doi.org/10.1007/BF01067955

Norman, M., Garcia, O. and Bennett, V. (2004). Rhenium and chalcophile elements in basaltic glasses from Ko'olau and Moloka'i volcanoes: Magmatic outgassing and composition of the Hawaiian plume. Geochim. Cosmochim. Acta 68(18), 3761–3777. https://doi.org/10.1016/j.gca.2004.02.025

Plechov, P. Y., Blundy, J. D., Nekrylov, N., Melekhova, E., Shcherbakov, V. D. and Tikhonova, M. S. (2015). Petrology and volatile content of magmas erupted from Tolbachik Volcano, Kamchatka, 2012-13. J. Volcanol. Geotherm. Res. 307(August 2013), 182–199. https://doi.org/10.1016/j.jvolgeores.2015.08.011

Rubin, K. (1997). Degassing of metals and metalloids from erupting seamount and mid-ocean ridge volcanoes: Observations and predictions. Geochim. Cosmochim. Acta 61(17), 3525–3542. https://doi.org/10.1016/S0016-7037(97)00179-8

Symonds, R. B., Rose, W. I., Bluth, G. J. S. and Gerlach, T. M. (1994). Volcanic gas studies: methods, results and applications. In: Volatiles in Magmas., Carroll, M.R.:Hollaway, J.R. (Editors), Mineralogical Society of America, Washington D.C., 1-66.

Verma, S. P., Rosales-Rivera, M., Díaz-González, L. and Quiroz-Ruiz, A. (2017). Improved composition of hawaiian basalt BHVO-1 from the application of two new and three conventional recursive discordancy tests. Turk. J. Earth Sci. 26(5), 331–353. https://doi.org/10.3906/yer-1703-16

Zelenski, M., Fischer, T. P., de Moor, J. M., Marty, B., Zimmermann, L., Ayalew, D., Nekrasov, A. N. and Karandashev, V. K. (2013). Trace elements in the gas emissions from the Erta Ale volcano, Afar, Ethiopia. Chem. Geol. 357, 95–116. https://doi.org/10.1016/j.chemgeo.2013.08.022

Zelenski, M., Malik, N. and Taran, Y. A. (2014). Emissions of trace elements during the 2012-2013 effusive eruption of Tolbachik volcano, Kamchatka: Enrichment factors, partition coefficients and aerosol contribution. J. Volcanol. Geotherm. Res. 285, 136–149. https://doi.org/10.1016/j.jvolgeores.2014.08.007

Zoller, W. H., Parrington, J. and Phelan Kotra, J. (1983). Iridium enrichment in airborne particles from Kilauea volcano: January 1983. Science 222, 4–7. https://doi.org/10.1126/science.222.4628.1118

Tables

Table 1. Notation list.

Symbol	Definition	Unit
	Symbols	
a	distance	
A	area	
C	concentration	
D	diffusivity	m^2/s
D_W	diffusivity of water	m^2/s
D_X	diffusivity of a component X	m^2/s
$\bar{D}_X$	relative diffusion coefficient of component X, $\bar{D}_X = D_X / D_W$	
EF	enrichment factor	
Kd	equilibrium mass partition coefficient	
K_d*	observed mass partition coefficient	
Kv	volume partition coefficient	
η	dynamic viscosity	Pa·s
q	specific diffusion flux	$kg/(s \cdot m^2)$
r	bubble radius	m
$R\rho$	ratio of partial densities	
t	time	s

u	velocity	m/s
ΔC_W	supersaturation in water	
ρ	density	kg/m^3
	Indices	
eq	equilibrium	
fl	fluid	
meas	measured	
melt	melt	
R	reference element	
W	water	
X	component X	
	Dimensionless scaling parameters	
Pe	Peclet number	
Re	Reynolds number	

Table 2. Parameters of silicate melts on Kilauea and Tolbachik volcanoes.

Volcano	Kilauea	Tolbachik, the 2013 eruption	Note
Pressure at the melt surface, bar	0.9	0.85	1000 m asl for Kilauea 1400 m asl for Tolbachik
Melt composition	basalt[a]	basaltic trachyandesite[b]	a, Gladney and Roelandts, 1988; Verma et al., 2017. b, Zelenski et al., 2014; Plechov et al., 2015
Melt density, kg/m^3	2660	2700	
Fluid density, kg/m^3	0.216	0.184	Calculated taking into account the gas composition and T
Temperature, °C	1150 – 1175[a]	1065[b]	a, Cashman et al., 1994; Ault et al., 1961. b, Zelenski et al., 2014
Water content, wt. %	0.08-0.3[a]	0.18-0.34[b]	a, Cashman et al., 1994; Wallace and Anderson, 1997 b, this work; Plechov et al., 2015
Dynamic viscosity, η, at 0.3 wt. % H_2O, Pa·s	68	1160	Calculated according to Giordano et al., 2008
Diffusion coefficient of H_2O, m^2/s	2.19E-11	5.60E-12	Calculated according to Zhang et al., 2017
Diffusion coefficient of Na, m^2/s	2.59E-10	1.5E-10	Zhang et al., 2010
Diffusion coefficient of Fe, m^2/s	1.34E-12	3.8E-13	Zhang et al., 2010
Modal bubble radius, mm	0.25[a]	unknown	a, Chevrel et al., 2018
Reynolds number for a 1 mm bubble	1E-05	3.6E-08	Calculated
Reynolds number for a 10 mm bubble	0.01	3.6E-05	Calculated

Table 3. Equilibration time for element concentrations in a bubble after the transition from the decompression – diffusion growth mode to diffusion growth mode, for some elements in Tolbachik melt.

Element	Diffusivity, cm^2/s	C(melt), ppm wt.	C(gas), ppm wt.	Equilibration time, s
Te	3.60E-09	0.004	0.33	31
Cl	1.10E-08	595	24740	4.5
Tl	2.10E-09	0.12	1.7	4.4
Cd	1.10E-09	0.12	0.66	1.3
Br	2.10E-08	4.6	48	0.24
Pb	5.10E-09	7.5	0.74	8.9E-05
Cs	2.50E-09	2.14	0.102	4.2E-05
K	6.30E-08	20643	249	1.1E-07

Equilibration time is estimated for a 1-mm model bubble using numerical calculations as described in Electronic Annex 1 Part 2, with the exception of tellurium, which equilibration time was estimated from the thickness of the diffusion boundary layer.

Table 4. General information on the volcanoes under the study.

Volcano, reference	Location	Tectonic setting	Degassing mode	Method of gas sampling	Major gas species, mol. %					
					H_2O	CO_2	SO_2	H_2S	HCl	HF
Ambrym[1]	New Hebrides	Island arc	Open vent, lava lake	Remote, Multigas, filters	95.1	3.0	1.5	0.015	0.25	0.11
Erta-Ale[2]	Ethiopia	Rift/hotspot	Lava lake, subsurface	Remote, direct sampling,	62.6	20.7	10.9	0.54	0.34	0.47
Etna[3]	Mediterranean	Island arc, complex	Open vent	Remote, filters	92.7	9.56	2.86	n.d.	1.43	0.48

Kilauea[4]	Hawaii	Hotspot	Lava flows, Lava tubes	Remote, direct sampling,	81.7	3.38	12.3	0.84	0.21	0.19
Masaya[5]	Central America	Continental arc	Open vent, subsurface lava lake	Remote, filters	92.9	4.37	1.81	n.d.	0.80	0.16
Tolbachik[6]	Kamchatka	Continental arc	Lava flows, Lava tubes	Direct sampling,	92.4	3.48	2.27	n.d.	1.37	0.49

Note: References are provided for the gas composition data: 1 – Allard et al., 2016; 2 – Zelenski et al., 2013; Giggenbach and Le Guern, 1976; 3 – Gerlach, 1979; Aiuppa et al., 2004; Shinohara et al., 2008, 4 – Gerlach and Graeber, 1985; Greenland, 1984; 5 – Duffell et al., 2003; 6 – Zelenski et al., 2014. n.d.: No data.

Table 5a. Apparent partition coefficients $Kd^* = C_X^{fl} / C_X^{m}$, calculated for the volcanic gas – silicate melt system. Elements with low uncertainties (typically < ± half an order of magnitude, < ±0.5 on the log scale). Osmium and iridium are also shown here.

Element	Kd* for arc: average (min-max)	log Kd* for arc	Kd* for rift/hotspot: average (min-max)	log Kd* for rift/hotspot
S	650 (322-922)	2.81±0.30	1105 (1044-1167)	3.04±0.02
Te	77 (71-81)	1.88±0.03	556 (425-728)	2.75±0.12
Se	52 (49-56)	1.72±0.03	129 (51-329)	2.11±0.41
Cl	32 (26-42)	1.51±0.11	30 (23-39)	1.48±0.06
Tl	23 (14-54)	1.35±0.38	3.6 (1.7-7.7)	0.56±0.33
Re	21 (17-25)	1.31±0.09	40 (39-42)	1.60±0.03
Os			12	1.09
Bi	12 (9-15)	1.07±0.12	8.9 (5.3-15.0)	0.95±0.23
Br	8.4 (6.8-10.4)	0.93±0.09	6.6 (3.3-13.3)	1.07±0.17
F	6.9 (4.3-9.2)	0.84±0.20	9.6 (8.4-11.0)	0.82±0.06
Cd	6.3 (5.2-7.1)	0.80±0.08	23 (15-33)	1.35±0.17
Au	3.1 (2.5-3.9)	0.49±0.10	1.5	0.19
In	1.7 (1.1-2.8)	0.24±0.20	1.0 (0.4-2.1)	-0.02±0.34
As	0.79 (0.32-4.7)	-0.10±0.77	1.14 (0.88-1.5)	0.06±0.11
Ag	0.44 (0.14-1.4)	-0.35±0.50	0.37	-0.43
Pt	0.26 (0.25-0.27)	-0.58±0.01	0.17	-0.76
Pb	0.23 (0.09-0.83)	-0.64±0.55	0.63 (0.54-0.73)	-0.20±0.06
Ir			0.13	-0.88
Cu	0.11 (0.04-0.42)	-0.97±0.51	0.023 (0.014-0.037)	-1.64±0.21
Cs	0.103 (0.05-0.34)	-0.99±0.52	0.049 (0.035-0.068)	-1.31±0.14
Zn	0.048 (0.028-0.089)	-1.32±0.27	0.10 (0.054-0.19)	-1.00±0.27

Mo	0.040 (0.024-0.070)	-1.40±0.25	0.080 (0.070-0.085)	-1.10±0.05
Rb	0.036 (0.018-0.117)	-1.44±0.51	0.012 (0.05-0.032)	-1.92±0.42
K	0.025 (0.012-0.051)	-1.60±0.30	0.011 (0.07-0.016)	-1.97±0.16
Li	0.012 (0.009-0.016)	-1.91±0.12	0.011 (0.04-0.034)	-1.95±0.48
Na	0.0101 (0.008-0.013)	-1.99±0.10	0.0036 (0.002-0.0065)	-2.44±0.26
Fe	0.00039 (0.00012-0.00079)	-3.41±0.52	0.00015 (0.00006-0.00038)	-3.83±0.41
V	0.00028 (0.00009-0.00128)	-3.55±0.66	0.00007 (0.00005-0.00011)	-4.13±0.16
Ce	0.00026 (0.00007-0.00094)	-3.58±0.56	0.00005	-4.33

Table 5b. Apparent partition coefficients $Kd^* = C_X^{fl} / C_X^m$, calculated for the volcanic gas – silicate melt system. Elements with high uncertainties (typically > ± half an order of magnitude, > ±0.5 on the log scale).

Element	Kd* for arc: average (min-max)	log Kd* for arc	Kd* for rift/hotspot: average (min-max)	log Kd* for rift/hotspot
Sb	3.0 (0.17-255)	0.48±1.93	0.16 (0.092-0.29)	-0.79±0.25
Sn	0.68 (0.061-7.6)	-0.17±1.05	0.56 (0.30-1.1)	-0.25±0.27
Hg	0.24 (0.021-2.8)	-0.62±1.07	0.0035	-2.46
Cr	0.038 (0.0018-0.80)	-1.42±1.32	0.00067 (0.000025-0.018)	-3.17±1.43
U	0.030 (0.0088-0.12)	-1.52±0.61	0.0024	-2.62
Ge	0.019	-1.72	0.086 (0.044-0.17)	-1.06±0.29
Ta	0.017	-1.78	0.00060 (0.00014-0.0026)	-3.22±0.64
B	0.011	-1.95	0.71 (0.058-8.8)	-0.15±1.09
W	0.010	-2.00	0.0073 (0.0023-0.024)	-2.13±0.51
Co	0.0038 (0.00047-0.10)	-2.42±1.43	0.00060 (0.00029-0.0012)	-3.22±0.32
Be	0.0033 (0.00026-0.042)	-2.48±1.10	0.0031 (0.00034-0.027)	-2.52±0.95
Ti	0.0030	-2.53		
Al	0.0022 (0.00004-0.046)	-2.66±1.69	0.00060	-3.22
La	0.0019 (0.00029-0.010)	-2.71±0.82	0.00050	-3.30
Nb	0.0015	-2.81	0.00014	-3.87
Th	0.0015 (0.00070-0.0030)	-2.84±0.32	0.00013 (0.000022-0.00076)	-3.89±0.77
Mn	0.0013 (0.00041-0.011)	-2.88±0.92	0.00011 (0.00011-0.00012)	-3.94±0.02
Ga	0.0012 (0.00007-0.034)	-2.94±1.47	0.0011 (0.0011-0.0012)	-2.94±0.02
Ni	0.00095	-3.02	0.0079 (0.00044-0.14)	-2.10±1.26

Ba	0.00080 (0.00008-0.0064)	-3.06±1.04	0.00039 (0.00011-0.013)	-3.41±0.54
Ca	0.00043 (0.00011-0.0017)	-3.37±0.59	0.00037	-3.43
Sr	0.00032 (0.00006-0.0017)	-3.50±0.73	0.00010	-3.99
Y	0.00027	-3.56	0.00025	-3.61
Sc	0.00026	-3.59		
Si	0.00025	-3.60	0.00043	-3.36
Eu	0.00023	-3.64	0.000076	-4.12
P	0.00016	-3.79	0.00048 (0.00019-0.0013)	-3.31±0.41
Hf	0.00016	-3.81	0.00010 (0.000027-0.00038)	-3.99±0.58
Zr	0.00010	-4.00	0.00068	-3.17

Table 6. Comparison of the element speciation in volcanic gas and *Kd** for HCl-rich and S-rich gases

Element	Predominant gaseous species	log *Kd* for arc gases (HCl-rich)	log *Kd* for rift/hotspot gases (sulfur-rich)	Δ log *Kd* (arc – rift/hotspot)
Cr	$CrCl_2$, $CrCl_2O_2$, $CrCl_3$, CrO_2,	-1.42	-3.17	1.75
Mn	$MnCl_2$, MnF_2, Mn^0	-2.88	-3.94	1.06
Th	Fluorides/chlorides?	-2.84	-3.89	1.05
Co	$CoCl_2$, $Co(OH)_2$	-2.42	-3.22	0.80
Tl	TlCl, Tl_2Cl_2, TlI, TlBr, Tl^0	1.35	0.56	0.79
Cu	CuCl, Cu_2Cl_2, Cu_3Cl_3	-0.91	-1.64	0.73
V	VCl_3O, VCl_2, VO_2, VBr_4, VO	-3.55	-4.13	0.58
Rb	RbCl, Rb^0	-1.44	-1.92	0.48
Na	NaCl, Na_2Cl_2, NaOH, NaBr	-1.99	-2.44	0.45
Fe	$Fe(OH)_2$, $FeCl_2$, $FeCl_3$, FeF_3	-3.41	-3.83	0.42
K	KCl, K_2Cl_2, KOH, KBr	-1.60	-1.97	0.37
Cs	CsCl, CsOH, Cs^0	-0.99	-1.31	0.32
In	InCl, $InCl_2$, $InCl_3$, InBr	0.24	-0.02	0.26
W	H_2WO_4, WO_2Cl_2, WO_3	-2.00	-2.13	0.13

Bi	Bi^0, BiS, BiCl	1.07	0.95	0.12
Ag	AgCl, Ag^0, AgBr	-0.35	-0.43	0.08
As	$As(OH)_3$, AsS, As_2, As^0	-0.10	0.06	-0.16
Zn	Zn^0, $ZnCl_2$, ZnS	-1.32	-1.00	-0.32
Se	H_2Se, Se^0, Se_2, SeO	1.72	2.11	-0.39
Pb	PbS, $PbCl_2$, Pb^0	-0.64	-0.20	-0.44
Cd	Cd^0, CdS, $CdCl_2$	0.80	1.35	-0.55
Te	Te^0, Te_2, H_2Te, TeO	1.88	2.75	-0.87
Au	AuS, AuH, Au^0	0.49	0.19	0.3
Mo	H_2MoO_4, MoO_2Cl_2, MoO_3	-1.40	-1.1	-0.3

Highlights

Partition coefficients Kd for 58 elements are reported for volcanic gas – melt system
Observed partition coefficients are almost indistinguishable from equilibrium ones
Element properties, S and Cl contents and fO2 of the gas are factors to determine Kd

Declaration of interests

☒ The authors declare that they have no known competing financial interests or personal relationships that could have appeared to influence the work reported in this paper.

☐The authors declare the following financial interests/personal relationships which may be considered as potential competing interests: